

UNIVERSIDAD AUTÓNOMA DE MADRID

FACULTY OF SCIENCES

Multimessenger signatures of particle acceleration by black holes

Alejandro Svyatkovskyy Kholyavka

Director

Dr. Rafael Alves Batista

MSc Thesis in Theoretical Physics
Speciality in Astrophysics and Physics of the Cosmos

Academic year 2023-2024

Day of the defense: September 9th, 2024

Examiners of the defense:

Prof. Dr. Ángeles Díaz

Prof. Dr. Violeta González

Prof. Dr. Tomás Hough

Prof. Dr. Alexander Knebe

Моїм батькам, Сюзані та Джорджу

Acknowledgements

Prior to the reader who has this work in their hands delving into the intricacies of particle acceleration, black holes, and the fascinating Multimessenger world, I would like to interrupt their reading for a few lines to thank the people who have supported and made this work possible, as without them, it would not be the same.

First of all, to Rafa, who took on the task of mentoring me for a few months and with whom I have spent countless hours discussing whether what we were scheming could be true or not. Thanks to him, I have been able to improve both as a student and as a person and hopefully one day we will work together in some Multimessenger stuff.

Next, I would like to thank Máximo Bañados, Joseph Silk, and Stephen West for the fruitful discussions that have added significant value to this work, as well as Masashi Kimura for the email exchanges that cleared up a sea of doubts while I was writing this document.

Of course, I cannot forget my parents, who represent a fundamental part of my life and to whom I will always be grateful for the effort they have made to get me here.

Finally, I would like to dedicate a few lines to Susana, my favorite person. She is the one who supported me when I couldn't go on and gave me the strength to keep going until the end. And, as Cruz Cafuné once said: "For me, love is the most important thing, it is the common point, the nexus, it is what articulates everything that is alive." This is what she represents to me, and that is why I dedicate this work to her.

Abstract

In this work, we analyze the center-of-mass (COM) energy of particle collisions near black hole (BH)s in Schwarzschild and Kerr spacetimes to evaluate their potential to produce ultra-high-energy cosmic ray (UHECR)s. While the Schwarzschild BH achieves limited COM energy that cannot account for UHECRs, the Kerr spacetime allows for divergent COM energy near its extremal event horizon. Although the COM energy can reach very high levels near the event horizon of an extremal Kerr BH, the energy of the escaping particles is limited, reducing the overall efficiency of the process. The efficiency varies depending on the type of escaping particle, being higher for photons than for massive particles. This indicates that while the Bañados-Silk-West (BSW) mechanism can clear the way for high-energy (HE) collisions, it is not sufficient to fully explain the origin of UHECRs.

The study reveals that cascading interactions in HE environments can highly amplify particle energy, which is a key process in astrophysical particle acceleration and Multimessenger context. These cascades occur when an initial interaction, such as a particle collision near a BH, triggers a series of secondary reactions, producing new particles that, in turn, interact with their surroundings. Our study suggests that while the BSW mechanism does not resolve the UHECR mystery, it opens new avenues for exploring extreme physical conditions around BHs, offering insights into Dark Matter (DM) interactions and HE phenomena.

Additionally, the strong gravitational fields around BHs significantly increase the local density of DM, boosting the likelihood of interactions and annihilation events. These HE environments create conditions for unique annihilation signals that are difficult to observe elsewhere, providing indirect evidence of DM and insights into its properties beyond the Standard Model. Such interactions can alter the energy distribution of particles, potentially leading to resonances that affect annihilation pathways and produce distinct astrophysical signatures.

Future work will extend this analysis beyond the equatorial plane (eq. plane) and validate these models through *CRPropa* simulations integrated with observational data, providing a crucial step toward understanding HE cascades in astrophysical contexts. This approach not only helps in exploring the extreme conditions near BHs but also offers a window into the elusive nature of DM through its gravitationally enhanced interactions in these regions.

Keywords: UHECRs, black hole, center-of-mass, BSW mechanism, Multimessenger, interactions.

Resumen

En este trabajo, analizamos la energía del centro de masa (**COM**) de las colisiones de partículas cerca de agujeros negros (**BHs**) en los espaciotiempos de Schwarzschild y Kerr para evaluar su potencial en la producción de rayos cósmicos de ultra alta energía (**UHECRs**). Mientras que el **BH** de Schwarzschild alcanza una energía de **COM** limitada que no puede explicar los **UHECRs**, el espaciotiempo de Kerr permite una energía de **COM** divergente cerca de su horizonte de eventos extremal. Aunque la energía de **COM** puede alcanzar niveles muy altos cerca del horizonte de un **BH** de Kerr extremal, la energía de las partículas que escapan es limitada, reduciendo la eficiencia global del proceso. La eficiencia varía según el tipo de partícula que escapa, siendo mayor para los fotones que para las partículas masivas. Esto indica que, aunque el mecanismo de Bañados-Silk-West (**BSW**) puede facilitar colisiones de alta energía (**HE**), no es suficiente para explicar completamente el origen de los **UHECRs**.

El estudio revela que las interacciones en cascada en entornos de **HE** pueden amplificar considerablemente la energía de las partículas, lo cual es un proceso clave en la aceleración de partículas astrofísicas y en el contexto Multimensajero. Estas cascadas ocurren cuando una interacción inicial, como una colisión de partículas cerca de un **BH**, desencadena una serie de reacciones secundarias, produciendo nuevas partículas que, a su vez, interactúan con su entorno. Nuestro estudio sugiere que, aunque el mecanismo **BSW** no resuelve completamente el misterio de los **UHECRs**, abre nuevas vías para explorar condiciones físicas extremas alrededor de los **BHs**, ofreciendo perspectivas sobre las interacciones de la materia oscura (**DM**) y fenómenos de **HE**.

Además, los intensos campos gravitacionales alrededor de los **BHs** aumentan significativamente la densidad local de **DM**, incrementando la probabilidad de interacciones y eventos de aniquilación. Estos entornos de **HE** crean condiciones para señales de aniquilación únicas que son difíciles de observar en otros contextos, proporcionando evidencia indirecta de la **DM** y ofreciendo perspectivas sobre sus propiedades más allá del Modelo Estándar. Dichas interacciones pueden alterar la distribución de energía de las partículas, lo que podría llevar a resonancias que modifiquen las rutas de aniquilación y produzcan firmas astrofísicas distintivas.

Trabajos futuros ampliarán este análisis más allá del plano ecuatorial y validarán estos modelos mediante simulaciones con *CRPropa* integradas con datos observacionales, proporcionando un paso crucial hacia la comprensión de las cascadas de **HE** en contextos astrofísicos. Este enfoque ofrece una ventana hacia la naturaleza esquiva de la **DM** a través de sus interacciones gravitacionales mejoradas en estas regiones.

Palabras clave: *UHECRs, agujero negro, centro de masa, BSW, Multimensajero, interacciones.*

Contents

1 Multi-Messenger Astronomy	1
1.1 Cosmic rays	1
1.2 Gamma rays	2
1.3 Neutrinos	2
1.4 Gravitational Waves	3
2 Particle interactions	4
2.1 Photonuclear interactions	4
2.1.1 Bethe-Heitler pair production	4
2.1.2 Photomeson production	5
2.1.3 Nuclear photodisintegration	6
2.2 Electromagnetic interactions	6
2.2.1 Breit-Wheeler pair production	6
2.2.2 Inverse Compton scattering	7
2.3 Adiabatic cosmological losses	7
3 Particle acceleration in Astrophysics	8
3.1 Origin of UHECRs	8
3.2 Overall restrictions	8
3.2.1 The Hillas criterion	9
3.3 Mechanisms of acceleration	10
3.3.1 Diffusive acceleration mechanisms	10
3.3.2 Inductive acceleration mechanisms	11
3.4 Fermi Acceleration Mechanisms	11
3.4.1 Second-Order Fermi Acceleration	11
3.4.2 First-Order Fermi Acceleration	12
4 Bañados-Silk-West mechanism	13
4.1 Schwarzschild black hole	14
4.2 Kerr black hole	17
5 Efficiency of the BSW mechanism	19
5.1 Particle interactions	19
5.1.1 Interactions with an escaping photon	20
5.1.2 Interactions with an escaping massive particle	21

6 Discussion	23
7 Summary	25
A Energy losses of different particle interactions	30
B Geometrized unit system	32
C Resolution of expression (4.12) at the event horizon	33
D Angular momentum range for the BSW process in Kerr spacetime	35
E Mathematical treatment for the efficiency of the BSW mechanism	37
F Maximal energies and efficiencies for escaping massless particle's cases	40
F.1 Outgoing pair annihilation (MMP+)	40
F.2 Ingoing Compton Scattering (PMP-)	40
F.3 Outgoing Compton Scattering (PMP+)	41
F.4 Ingoing inverse Compton scattering (MPP-)	42
F.5 Outgoing inverse Compton scattering (MPP+)	42
G Maximal energies and efficiencies for escaping massive particle's cases	44
G.1 Ingoing elastic scattering (MMM-)	44
G.2 Ingoing inverse Compton scattering (MPM-)	45
G.3 Outgoing inverse Compton scattering (MPM+)	45
G.4 Ingoing photomeson production (PMM-)	46
G.5 Outgoing photomeson production (PMM+)	47

List of Figures

1.1	How do CRs , γ -rays and neutrinos interact with Earth's atmosphere?	2
1.2	Where is the Universe opaque to photons?	3
2.1	The CR energy spectrum	5
3.1	The Hillas diagram	10
3.2	Diffusive and inductive acceleration mechanisms	11
3.3	Fermi acceleration mechanisms	12
4.1	Schemes for the BSW mechanisms	13
4.2	Behavior of a particle near a Schwarzschild BH	16
4.3	Behavior of a particle near a Kerr BH	18
5.1	Energy extraction mechanisms near a Kerr BH	19
5.2	Efficiency of critical and subcritical particle collisions	21
5.3	Efficiency in collisions with escaping massive particles	22
A.1	Distribution of the attenuation length of different CR nuclei as a function of energy	30
A.2	Interaction rates for various processes	31
D.1	Behaviour of the effective potential near a Kerr BH.	35
E.1	Processes with <i>ingoing</i> and <i>outgoing</i> particles	37
E.2	Impact Parameter Conditions	38

List of Tables

5.1	Distribution of maximum energies and efficiencies obtained for the different particle interactions in which particle (3) is massless.	21
5.2	Distribution of maximum energies and efficiencies obtained for the different particle interactions in which particle (3) is massive.	22

List of Abbreviations

- AGN** active galactic nuclei
BH black hole
BSW Bañados-Silk-West
CMB Cosmic Microwave Background
COM center-of-mass
CR cosmic ray
DM Dark Matter
EAS extensive air shower
EM electromagnetic
EoM equations of motion
eq. plane equatorial plane
 γ -ray gamma-ray
GW gravitational wave
GZK Greisen-Zatsepin-Kuzmin
HE high-energy
ICS inverse Compton scattering
IS International System
LE low-energy
MM Multi-Messenger
UHECR ultra-high-energy cosmic ray
VHE very-high-energy

Multi-Messenger Astronomy

The human being has observed the sky and its stars since time immemorial, but until the mid-20th century, observations were mainly in the optical range. With the inclusion of instruments capable of observing the sky in new wavelengths such as radio or X-rays, a new era in Astronomy began, allowing for a broader scope.

As we moved into the 21st century, a wide variety of instruments were developed, giving the scientific community the opportunity to study an astrophysical object or event from the perspective of many cosmic messengers and wavelengths. And this is what Multi-Messenger (MM) Astronomy is about: the study of the Cosmos through the combination of information provided by various cosmic messengers [1].

These cosmic messengers can generally be classified into: cosmic ray (CR), gamma-ray (γ -ray), neutrino, and gravitational wave (GW). Each of them behaves differently on their journey from the astrophysical source to us, and this is what makes them fascinating—by combining them, we can unravel the mysteries of the Universe. [2].

1.1 Cosmic rays

CRs are one of the messengers on which we will focus our study, as they are primarily HE charged particles [2]. They travel at speeds close to the speed of light and usually come from our Sun or outside the galaxy [3]. An important feature of them is that when they exceed 1 EeV, they are considered UHECR [2]. They are mainly classified into:

- Primary CRs: Their origin is in astrophysical sources, and upon reaching Earth, they create an extensive air shower (EAS) in the atmosphere by interacting with air molecules.
- Secondary CRs: These interactions can occur either in the atmosphere or in space, due to processes such as photodisintegration. As shown in Figure 1.1, we can distinguish between electromagnetic (EM) cascades (producing γ -rays) and hadronic cascades (creating muons and neutrinos) [3].

On the other hand, due to their charge, as they travel through the Universe, they suffer deflection by all kinds of magnetic fields present, making it impossible to trace them back to their original source. This is one of the reasons why it is necessary to study objects using multiple messengers [3].

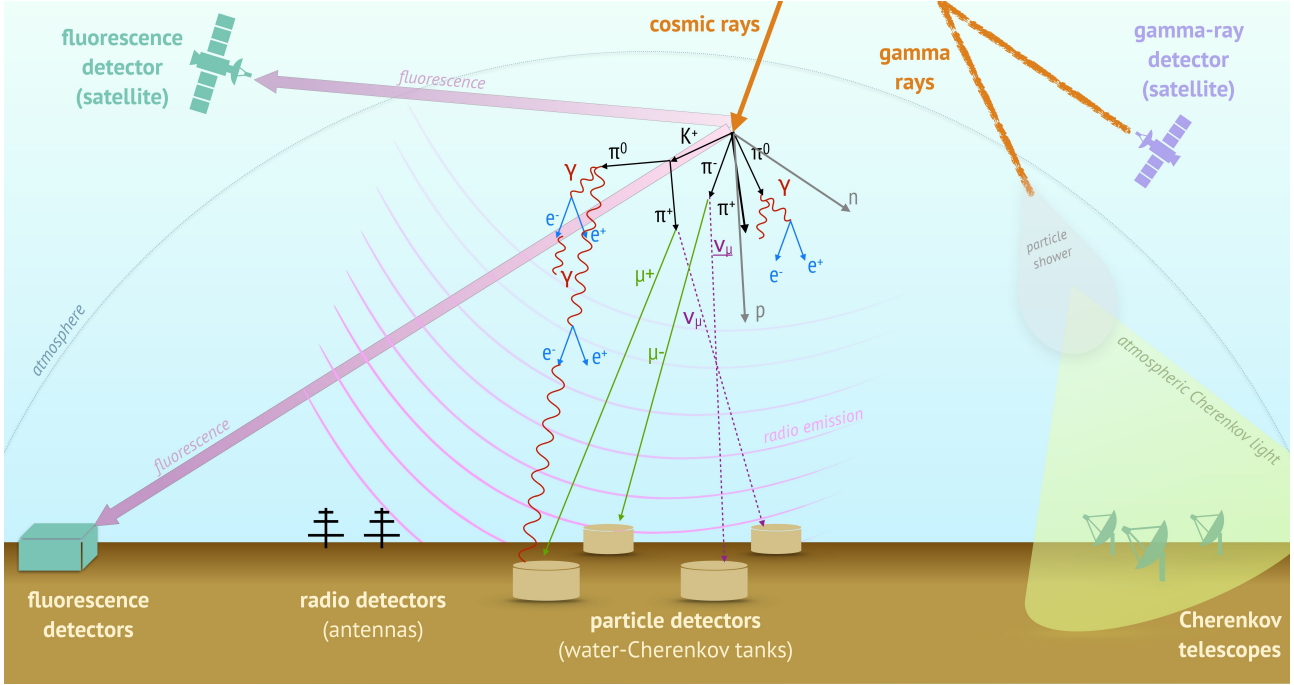


Figure 1.1: The illustration shows how CRs, γ -rays and neutrinos interact with Earth's atmosphere, leading to the production of secondary particles and various types of emissions. It highlights the different methods used to detect these particles, including ground and satellite-based fluorescence detectors, antennas for radio detection, water-Cherenkov tanks for particle detection, and Cherenkov telescopes that capture atmospheric Cherenkov light, all of which are essential in studying HE particle showers [4].

1.2 Gamma rays

EM radiation is also one of the counterparts in MM Astronomy. γ -rays are its most energetic form and can range from a few hundred keV to energies above PeV. Any photon with energy greater than 100 keV is considered a γ -ray [2].

γ -rays are not deflected by magnetic fields, but when they interact with a background photon, pair production occurs [5]

$$\gamma + \gamma_{bg} \rightarrow e^+ + e^- \quad (1.1)$$

This results in an electron-positron pair, which can be affected by magnetic fields. Additionally, if either of these particles interacts with another background photon, we have inverse Compton scattering (ICS) (similar to the Compton effect [6]).

$$e^\pm + \gamma_{bg} \rightarrow e^\pm + \gamma, \quad (1.2)$$

which produces a photon that will continue its journey. This forms what is known as the Cosmic γ -ray Horizon¹ [2].

1.3 Neutrinos

As mentioned earlier, we cannot determine the origin of the CRs that reach Earth, but we can use neutrinos to trace their source. This is because HE neutrinos can be produced near the source

¹Located at $z = 1$ for $E \sim 1$ GeV and at $z = 0$ for $E \sim 300$ GeV (for interactions with the Extragalactic Background Light) [7].

through interactions of CRs [3]. Due to their electrically neutral and weakly interacting nature, neutrinos almost² do not interact with any background fields, making them ideal for identifying the astrophysical source [2].

On the other hand, as we can see in Figure 1.2, the Universe is completely opaque to photons, which makes the use of neutrinos necessary to study the Universe at HEs [8].

1.4 Gravitational Waves

The last messenger we will mention are GWs. This counterpart is completely different from the others as it is of a gravitational type. It is a perturbation in spacetime resulting from the acceleration of massive astrophysical objects [3]. They also differ in detection because they record amplitudes and phases that contain information about the origin, rather than particles as with the others [2].

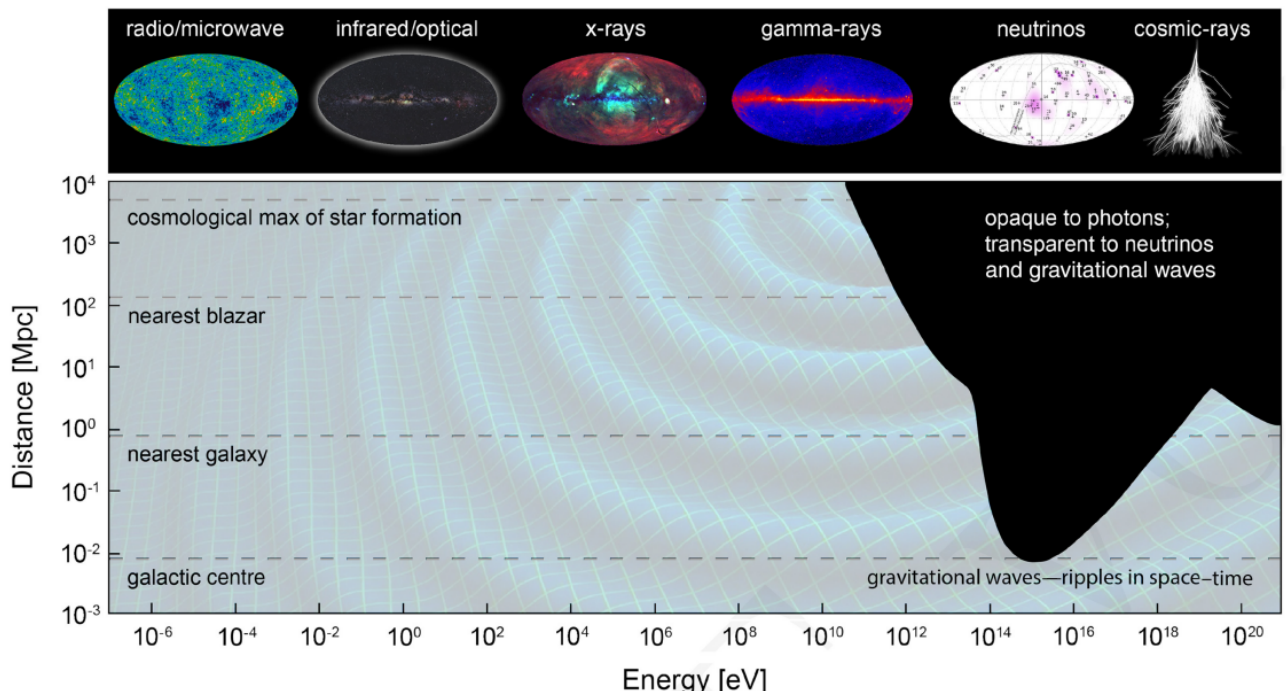


Figure 1.2: The distance at which the Universe becomes opaque to EM radiation limits the observation of the most energetic cosmic events. However, GWs and neutrinos can pass through the Universe unobstructed, making them ideal for studying HE phenomena [8].

²Because their mean free path is many times the size of the observable Universe.

2

Particle interactions

In our study, we will focus predominantly on the interactions of particles that are paramount to our research, given the nature of the particles under investigation. These interactions serve as pivotal elements shaping our understanding and analysis, guiding us towards comprehensive insights into the behavior and properties of the particles in question. The propagation of particles throughout the Universe is more significantly affected by EM radiation through a variety of processes that will be explained below.

One of the most relevant features we can find in the interaction between particles is the interaction rate of a process (λ^{-1}). Let's imagine an interaction between a cosmic messenger and a background photon; the interaction rate could be determined as follows [2]

$$\lambda^{-1}(E, z) = \frac{1}{8\beta E^2} \int_{\varepsilon_{min}(E)}^{+\infty} \frac{1}{\varepsilon^2} \frac{dn(\varepsilon, z)}{d\varepsilon} \int_{s_{min}}^{s_{max}(E, \varepsilon)} (s - m^2) \sigma(s) ds d\varepsilon, \quad (2.1)$$

where E is the energy of the messenger, z is the redshift, β is the velocity of the messenger

$$\beta = \sqrt{1 - \frac{m_e^2 c^4}{s}}, \quad \text{with} \quad s = m^2 c^4 + 2E\varepsilon(1 - \beta \cos(\theta)), \quad (2.2)$$

s is the squared COM energy, $\frac{dn}{d\varepsilon}(\varepsilon, z)$ is the distribution of background photon energies, and $\sigma(s)$ is the cross-section [2]. The equation (2.1) is plotted for a series of interactions in Appendix A.

2.1 Photonuclear interactions

Photonuclear interactions represent the process between any nucleus and a background photon, leading to a diverse range of possible outcomes



where X is the element's symbol, A is its mass number¹ and Z is its atomic number²

2.1.1 Bethe-Heitler pair production

The first possibility that arises is the production of electron-positron pairs [9]



¹The sum of the number of protons and neutrons.

²The number of protons.

This process is known as Bethe-Heitler pair production and may remind us somewhat of Bremsstrahlung, but with a photon as the reactant [10].

This process will only be possible if, in the rest frame of the nucleus, the energy of the photon is greater than 1 MeV [2]. Additionally, if UHECRs are composed only of protons, a specific process might explain a particular pattern observed in the energy distribution of these cosmic rays, known as the *ankle* energy [11].

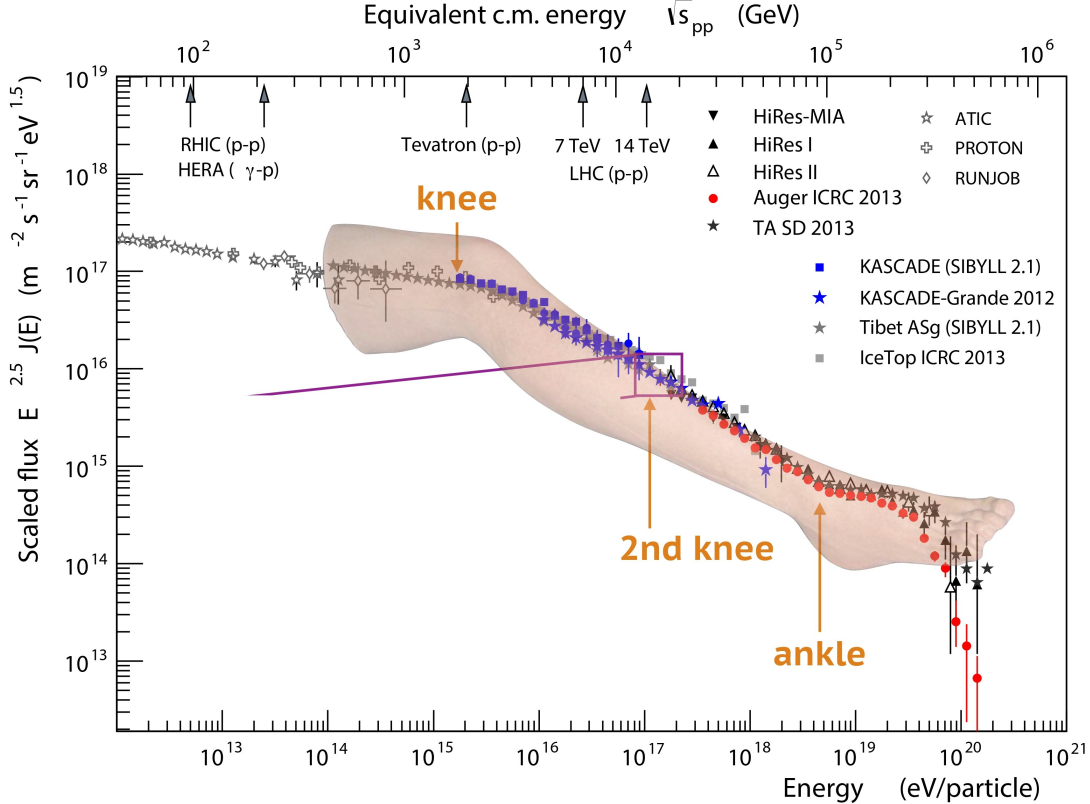


Figure 2.1: The CR energy spectrum, which displays the number of CRs detected as a function of their energy. The x-axis represents the energy of the CRs and the y-axis shows the flux of CRs (scaled to make the spectrum clearer) [12].

If we take a close look at Figure 2.1, we can observe a number of features:

- 1st knee: this is a noticeable bend in the spectrum around 10^{15} eV. It suggests a change in the behavior or origin of CRs, potentially indicating a transition from CRs produced within our galaxy to those of a different origin [13].
- 2nd knee: located at higher energies around 10^{17} eV. This feature represents another point where the slope of the spectrum changes, possibly suggesting another transition in the CR sources or the acceleration mechanism [13].
- Ankle: this feature appears around $10^{18.5}$ eV. The ankle marks a flattening in the spectrum, which may indicate a shift from galactic CRs to extragalactic CRs [13].

2.1.2 Photomeson production

Photomeson production is a very important process because it leads to the creation of photons and neutrinos, which are two types of messengers that allow us to explore and understand cosmic

phenomena. This process becomes particularly relevant when dealing with photons with very-high-energy (VHE), exceeding 1 GeV (in the rest frame of the nucleus)[10].

When UHECRs protons interact, they can induce a resonance (Δ^+). This resonance is a type of unstable intermediate state that decays into other particles. One way this decay occurs is when the resonance decays into a proton (p) and a neutral pion (π^0). The reaction can be written as follows [2]:



In another mode of decay, the resonance decays into a neutron (n) and a charged pion (π^+):



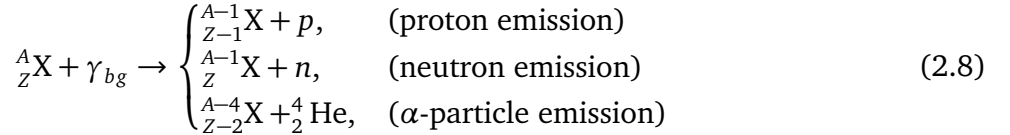
Once formed, the pions also decay. Neutral pions convert into photons while charged pions decay into neutrinos and charged leptons. This process has important implications because it contributes to the Greisen-Zatsepin-Kuzmin (GZK) cutoff [14, 15]. The GZK cutoff describes how HE protons are limited in the distance they can travel before losing energy due to interactions with the Cosmic Microwave Background (CMB) [2].

2.1.3 Nuclear photodisintegration

Another resulting product can be small constituents of the original nucleus



This phenomenon occurs when the photon energy exceeds 8 MeV and unfolds in two stages [10]. First, the atomic nucleus absorbs a photon and enters a HE excited state. This state is brief, as the nucleus soon relaxes to a stable state, releasing nucleons (protons or neutrons) in the process. Essentially, the nucleus absorbs energy, becomes excited, and emits nucleons upon stabilizing [16]. The possible products of photodisintegration are [10]:



2.2 Electromagnetic interactions

2.2.1 Breit-Wheeler pair production

This phenomenon occurs due to the interaction of two photons, resulting in the production of an electron-positron pair [5]



Because its cross-section has been extensively studied over time, we can identify it as [17]

$$\sigma_{PP} = \frac{3\sigma_T}{16} (1 - \beta^2) \left[(3 - \beta^4) \ln \left(\frac{1 + \beta}{1 - \beta} \right) - 2\beta (2 - \beta^2) \right], \quad (2.10)$$

where σ_T is the Thomson cross-section [10] and β has already been defined in expression (2.2).

In addition to the Breit-Wheeler pair production, there are more complex types of particle production. One of these is double pair production [18]. In this process, two HE photons interact to create two pairs of electron-positron. This is described by the following equation



2.2.2 Inverse Compton scattering

Another process we can encounter in the interaction between electrons and photons is the [ICS](#)

$$e^\pm + \gamma_{bg} \rightarrow e^\pm + \gamma, \quad (2.12)$$

which does not differ much from the original Compton effect [6]. The difference is that we are dealing with [HE](#) electrons and low-energy ([LE](#)) photons [10]. The expression for its cross-section is given by [17]

$$\sigma_{ICS} = \frac{3\sigma_T}{8\beta} \frac{m_e^2 c^4}{s} \left[\frac{2}{\beta(1+\beta)} (2+2\beta-\beta^2-2\beta^3) - \frac{1}{\beta^2} (2-3\beta^2-\beta^3) \ln\left(\frac{1+\beta}{1-\beta}\right) \right], \quad (2.13)$$

where $\beta \equiv (s-m_e^2)(s+m_e^2)$. If we are in the [LE](#) regime, where s approaches $m^2 c^4$, the previous expression becomes the Thomson cross-section.

Another interesting process is triplet production [19], which is the higher order version of [ICS](#). In this case, an electron interacts with a photon to produce an additional electron and a pair of electrons and positrons. The equation for this process is

$$e^\pm + \gamma_{bg} \rightarrow e^\pm + e^+ + e^-. \quad (2.14)$$

2.3 Adiabatic cosmological losses

As the Universe expands, all particles traveling over cosmological distances experience adiabatic energy losses due to this expansion, and it is possible to quantify this through [2]

$$\frac{1}{E} \frac{dE}{dt} = -H(z), \quad (2.15)$$

where E is the energy of the particles, t is time, $H(z)$ is the expansion rate, also known as the Hubble rate, and z is the redshift. Let's imagine for a moment that a particle is traveling towards us. If we consider only adiabatic losses, its energy upon arrival will be [2]

$$E_{final} = \frac{E_{initial}}{1+z_{source}}. \quad (2.16)$$

The Hubble rate changes over time, evolving faster now than in the early Universe, and it is expected to change even faster in the future. This behavior can be observed through the Friedmann equation [20]

$$H(z) = \frac{\dot{a}}{a} = H_0 \sqrt{\Omega_{m,0}(1+z)^3 + \Omega_{\Lambda,0}}, \quad (2.17)$$

where a is the scale factor, $H_0 = 67.36 \pm 0.54 \text{ km} \cdot \text{s}^{-1} \cdot \text{Mpc}^{-1}$ is the Hubble constant and, $\Omega_{m,0} = 0.3153 \pm 0.0073$ along $\Omega_{\Lambda,0} = 0.6847 \pm 0.0073$ represent the matter and vacuum densities that govern our Universe [21].

Particle acceleration in Astrophysics

The acceleration of **HE** particles is a fascinating and poorly understood phenomenon in Modern Physics. Despite the efforts of numerous researchers, it remains largely an enigma, with few satisfactory explanations. Among the hypotheses that have been proposed, many point towards an **EM** nature as the primary cause.

However, our interest lies in exploring a mechanism that challenges this predominant notion, specifically one of a gravitational nature. We have identified an approach that does not hold up under the **EM** hypothesis and that presents intriguing promises in understanding this fundamental process. It is precisely this divergence that motivates us to explore deeper into this area and to investigate further.

3.1 Origin of UHECRs

Previously, we have mentioned that the origin of **UHECRs** remains uncertain to this day. According to [22], we can have two scenarios (see [23] for a review):

- Top-down: the origin may be found in the decay of other particles that could be part of **DM** and other exotic entities such as magnetic monopoles, Z-bursts, cosmic strings, etc.
- Bottom-up: **UHECRs** undergo very strong accelerations due to magnetic fields in neutron stars or active galactic nuclei (**AGN**).

3.2 Overall restrictions

There is a wide variety of sources where **UHECRs** could have their astrophysical origin. These include **AGN**, tidal disruption events, galaxy clusters, γ -ray bursts, pulsars, binaries of **BHs**, and many more (see [2] for an individual review of each source). Therefore, it is necessary to impose constraints to consider or rule out potential sources [22, 24]:

- Configuration: while the particle is being accelerated, it cannot escape from the source.
- Capability: the source must be capable of accelerating particles in terms of energy.
- Energy dissipation: of course, the energy gain of the particle during acceleration must be greater than its energy losses due to radiation.
- Collision losses: the energy gain of the particle during acceleration must be greater than its losses due to interactions with other particles.

- Emission rate: the number density and power of the source must be consistent with the flux of **UHECRs** observed so far.
- Associated radiation: the flux of photons and neutrinos accompanying **UHECRs**, along with the flux of **LECRs**, must remain below the observed levels.

During this chapter, we will focus on explaining in detail the first and third constraints.

3.2.1 The Hillas criterion

In their study, Ptitsyna and Troitsky [24] discuss the possibility that a particle may escape from the source that is accelerating it. This would result in a pause in the increase of energy, which is a significant drawback. However, if the Larmor radius¹ (R_L) of the particle remains smaller than the size of the accelerator [22], the particle will not escape and will continue to gain energy. This is known as the Hillas criterion [25] and sets a maximum limit for the particle's energy.

$$E \leq E_H = qBR, \quad (3.1)$$

where E is the energy gained by the particle with charge q situated in a region of size R with magnetic field B [24].

Of course, during particle acceleration, there are energy losses due to radiation. This affects the maximum energy of the particles, which can be found as a solution to

$$\frac{dE^{(+)}}{dt} = -\frac{dE^{(-)}}{dt}, \quad (3.2)$$

where the left side represents the rate of energy gain and the right side represents the rate of energy loss. The first one equals to [24]

$$\frac{dE^{(+)}}{dt} = q\eta B, \quad (3.3)$$

while the second is

$$-\frac{dE^{(-)}}{dt} = \frac{2q^4}{3m^4}E^2\left(\left(\vec{E} + (\vec{v} \times \vec{B})\right)^2 - (\vec{E} \cdot \vec{v})^2\right) = \frac{2q^2}{3m^2(1-v^2)}\left(\vec{F}^2 - (\vec{F} \cdot \vec{v})^2\right). \quad (3.4)$$

In expressions (3.3) and (3.4), η is the efficiency, \vec{v} is the velocity of the particle, \vec{E} and \vec{B} are the electric and magnetic fields of the source, and \vec{F} is the force acting on the particle.

The maximum energy a particle can achieve is limited by two factors: the point where the energy gained equals the energy lost (3.2), and the Hillas criterion (3.1). The actual maximum energy is the minimum of these two values [24]:

$$E_{max} = \min \{E_H, E_{loss}\}. \quad (3.5)$$

This relationship is visualized in the Hillas plot (Figure 3.1), which identifies potential astrophysical sources of **UHECRs** based on their size and magnetic field strength. The plot's horizontal axis represents the size of the acceleration region, while the vertical axis shows the magnetic field strength. Colored regions indicate possible sources, such as **γ -ray bursts** and **AGN**. Diagonal lines show the thresholds below which particles cannot be accelerated to 10^{20} eV, differentiating between protons and iron (Fe) nuclei.

¹The Larmor radius is the distance over which a charged particle spirals when moving perpendicular to a uniform magnetic field.

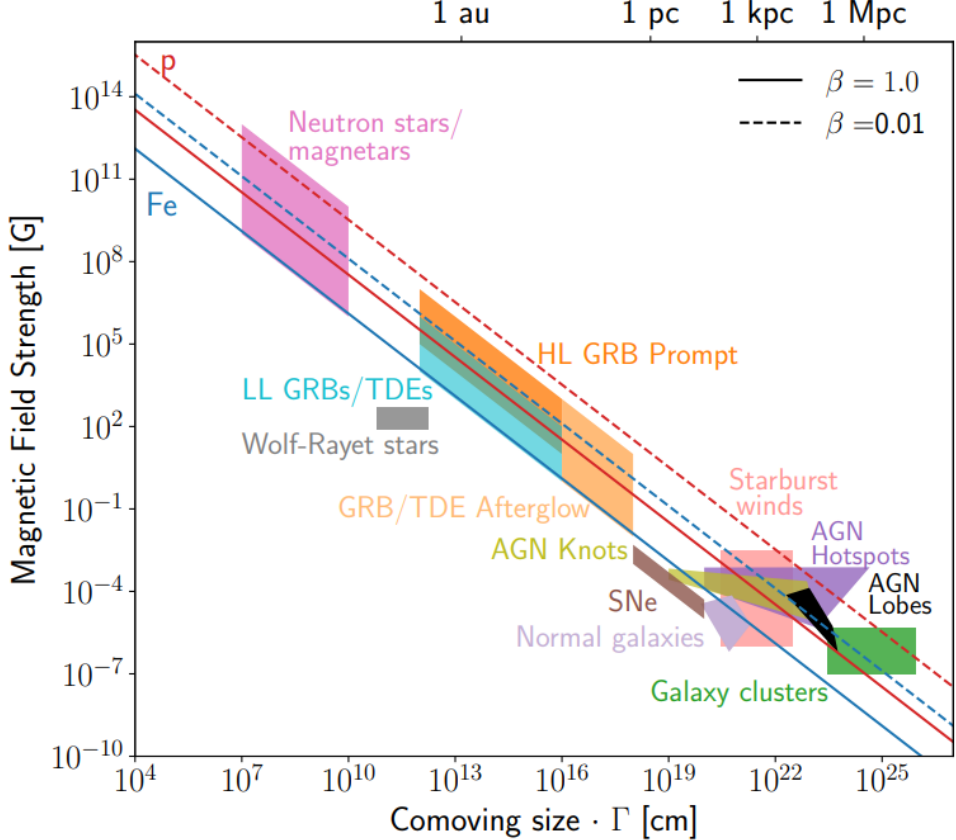


Figure 3.1: The Hillas diagram illustrates potential accelerators of UHECRs, highlighting regions where the size of the acceleration region and the strength of the magnetic field allow for particle acceleration. The diagonal lines indicate the limits for protons and iron nuclei, with continuous lines representing the maximum shock velocity ($\beta = 1$) and dashed lines for a lower shock velocity ($\beta = 0.01$) [2].

3.3 Mechanisms of acceleration

In this section, we will introduce the two main particle acceleration mechanisms in astrophysics. On one side, we have diffusive acceleration, which includes Fermi acceleration mechanisms. On the other side, there is inductive acceleration, divided into synchrotron losses and curvature losses.

3.3.1 Diffusive acceleration mechanisms

Here, particles are accelerated in *bursts* due to their interaction with magnetic fields [22], which leads to losses due to synchrotron radiation [24]:

$$-\frac{dE^{(-)}}{dt} = \frac{2q^2}{3R_L^2} \left(\frac{E}{m} \right)^4 = \frac{2q^4 E^2 B^2}{3m^4}, \quad (3.6)$$

where the maximum energy is given by:

$$E_d = \frac{3m^4 B^2 R^{-1}}{2q^4}. \quad (3.7)$$

3.3.2 Inductive acceleration mechanisms

This occurs when particles are continuously accelerated by an ordered field [22]. We have two types depending on the dominant radiation loss mechanism:

- Curvature: when $\vec{v} // \vec{E} // \vec{B}$, this situation arises. Here, the losses are governed by curvature [24]:

$$-\frac{dE^{(-)}}{dt} = \frac{2q^2}{3r^2} \left(\frac{E}{m}\right)^4, \quad (3.8)$$

where r represents the radius of curvature of the field lines. This results in a maximum energy of:

$$E_c = \left(\frac{3}{2}\right)^{\frac{1}{4}} \frac{mB^{\frac{1}{4}}R^{\frac{1}{2}}\eta^{\frac{1}{4}}}{q^{\frac{1}{4}}}. \quad (3.9)$$

- Synchrotron: in this case, the losses are determined by equation (3.6), leading to a maximum energy of [24]:

$$E_s = \left(\frac{3}{2}\right)^{\frac{1}{2}} \frac{m^2B^{-\frac{1}{2}}\eta^{\frac{1}{2}}}{q^{\frac{3}{2}}}. \quad (3.10)$$

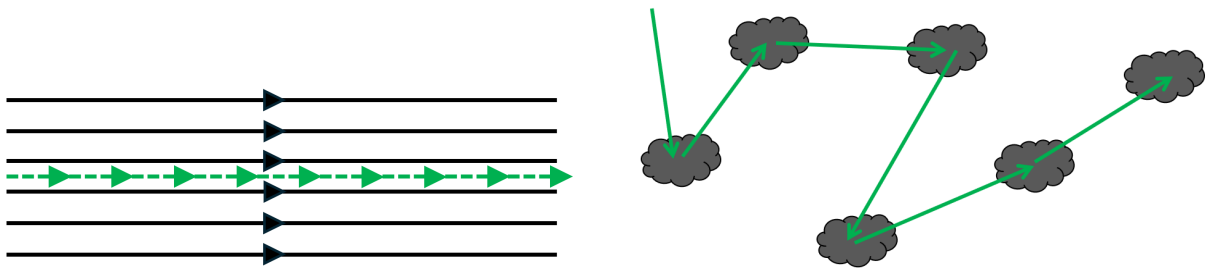


Figure 3.2: **Left:** inductive acceleration. **Right:** diffusive acceleration. Reproduced from [22].

3.4 Fermi Acceleration Mechanisms

3.4.1 Second-Order Fermi Acceleration

Let's imagine an environment with clouds that have a magnetic field. The second-order Fermi acceleration mechanism [26] accelerates particles to high energies in this environment. When a particle enters the cloud, it will have an energy (in the cloud's reference frame) given by [27, 28, 29]:

$$E'_i = \gamma E_i (1 - \beta \cos(\theta_i)), \quad \text{where } \gamma \equiv \frac{1}{\sqrt{1 - \beta^2}}, \quad \text{and } \beta \equiv \frac{v}{c}. \quad (3.11)$$

In this expression, γ represents the Lorentz factor. Additionally, E_i is the energy of the particle before colliding with the cloud, and θ_i is the incident angle. Subsequently, the energy when escaping the cloud is:

$$E_f = \gamma E'_f (1 - \beta \cos(\theta'_f)). \quad (3.12)$$

Since, in the reference frame of the cloud, the energies are equal ($E'_i = E'_f$) [29], the energy increment after each collision with the cloud will be:

$$\frac{\Delta E}{E} = \frac{E_f - E_i}{E_i} = \gamma \frac{E'_f}{E'_i} \left(1 - \beta \cos(\theta_i) + \beta \cos(\theta'_f) - \beta^2 \cos(\theta_i) \cos(\theta'_f)\right) - 1. \quad (3.13)$$

We seek the average energy gain, which can be calculated by averaging the angles in expressions (3.11) and (3.12) (see [29] for a complete analysis). The equation for the average energy gain is

$$\left\langle \frac{\Delta E}{E} \right\rangle \approx \frac{4}{3}\beta^2. \quad (3.14)$$

Since the energy gain is proportional to the square of β , this is treated as second-order Fermi acceleration. Now, considering the probability of the particle escaping the cloud [22]:

$$P_{esc} = \frac{4}{3}\beta^2, \quad (3.15)$$

we can find (see [28] for more details) that the energy spectrum is

$$N(E) = E^{-\alpha}, \quad (3.16)$$

where $N(E)$ stands for the particle number and α for the spectral index. Typically, this mechanism results in $\alpha \sim 2$ [30].

3.4.2 First-Order Fermi Acceleration

On the other hand, we have the first-order Fermi acceleration mechanism, which is necessary to achieve VHEs because the second-order mechanism cannot. In this case, the approach is similar to the second-order mechanism, but the cloud now moves with a relativistic velocity [31, 29].

The average energy gain in this case is [27, 28]:

$$\left\langle \frac{\Delta E}{E} \right\rangle \approx \frac{4}{3}\beta, \quad (3.17)$$

where we can see that it is proportional to β , allowing us to obtain VHEs, particularly when the velocities are high [29]. The differential energy spectrum is [29]

$$\frac{dN(E)}{dE} \propto E^\alpha, \quad (3.18)$$

and the escape probability is [22]

$$P_{esc} = \frac{4}{3}\beta. \quad (3.19)$$

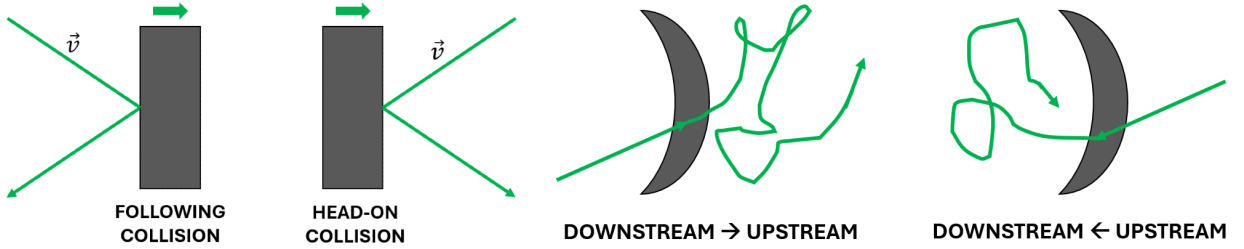


Figure 3.3: **Left:** second-order Fermi acceleration, where particles slowly gain energy by colliding with moving magnetic clouds. **Right:** first-order Fermi acceleration, where particles gain energy quickly by repeatedly crossing shock waves. Reproduced from [22].

Bañados-Silk-West mechanism

As previously mentioned, we have identified a gravitational-type mechanism that challenges the predominant view and does not align with the [EM](#) hypothesis, offering intriguing potential for understanding this fundamental process.

A [BH](#) is one of the sources that meets the constraints imposed in previous sections. These astrophysical objects are characterized by having a gravitational force so strong that they can trap even light. This enormous force means that any type of particle (whether charged or not) can be accelerated by the [BH](#), and therefore, they can be considered particle accelerators in the Universe [32].

Due to this, Máximo Bañados, Joseph Silk, and Stephen West conceived an idea that, for years, revolutionized the field of particle acceleration and energy extraction from [BHs](#). The [BSW](#) mechanism [33] suggests that it is possible to achieve arbitrarily [HE](#) in the [COM](#) frame of the collision of two particles around a rotating [BH](#). Although the original idea stems from the annihilation of [DM](#) particles at the galactic center [34], it can be extrapolated to a more general context involving fundamental particles.

The approach can be seen in Figure 4.1: two particles initially at rest at infinity falling into the [BH](#) and colliding near the horizon [33]. The idea from this point is to study the [COM](#) energy in various types of [BHs](#) to see how the mechanism behaves in different spacetimes.

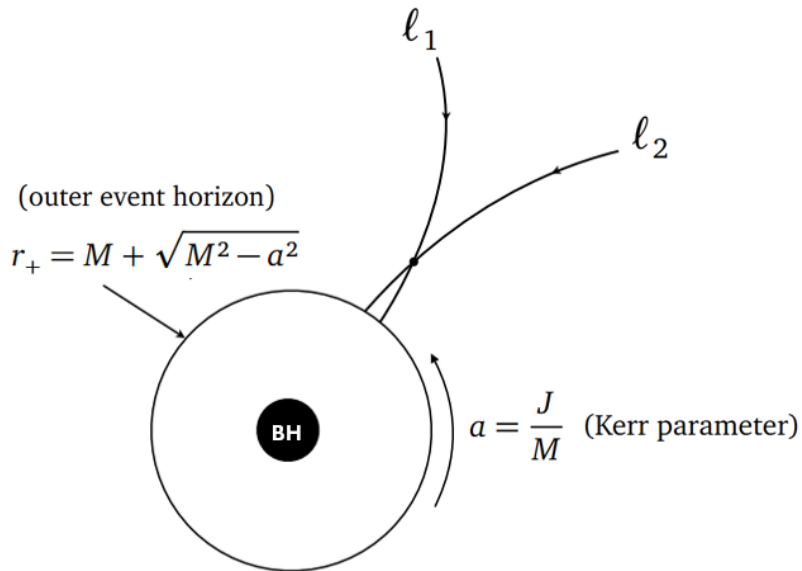


Figure 4.1: Illustration of the [BSW](#) mechanism for a Kerr [BH](#). Modified from [33]

4.1 Schwarzschild black hole

We will start with the simplest case, a Schwarzschild BH. It is known that the Schwarzschild spacetime is static and spherically symmetric. The static nature is defined by a Killing vector (ξ) and the symmetry by another Killing vector (η). Both give rise to two conserved quantities along any geodesic

$$E := -\xi \cdot \vec{p} \quad (4.1a)$$

$$L := \eta \cdot \vec{p}, \quad (4.1b)$$

where \vec{p} is the 4-momentum of the particle on the geodesic, and E is the conserved energy of the particle, while L is its conserved angular momentum [35].

The metric for this type of BH is written as (using a $(-, +, +, +)$ signature):

$$ds^2 = -\left(1 - \frac{2GM}{c^2r}\right)c^2dt^2 + \left(1 - \frac{2GM}{c^2r}\right)^{-1}dr^2 + r^2(d\theta^2 + \sin^2(\theta)d\varphi^2), \quad (4.2)$$

where G is the gravitational constant, M is the mass of the BH, and c is the speed of light.

In these coordinates, the aforementioned Killing vectors take a form¹ that makes the conserved quantities (4.1b) and (4.1b) become:

$$E = -\xi \cdot \vec{p} = -g_{\mu\nu}\xi^\mu p^\nu = -g_{t\nu}p^\nu = -p_t \quad (4.3a)$$

$$L = \eta \cdot \vec{p} = -g_{\mu\nu}\eta^\mu p^\nu = -g_{\varphi\nu}p^\nu = p_\varphi, \quad (4.3b)$$

where $g_{\mu\nu}$ represents the metric.

Now, we will investigate how a point particle behaves in this spacetime. To do this, we construct the Lagrangian:

$$\begin{aligned} \mathcal{L} &= \frac{1}{2}g_{\mu\nu}\frac{dx^\mu}{d\tau}\frac{dx^\nu}{d\tau} \\ &= \frac{1}{2}\left[-\left(1 - \frac{2GM}{c^2r}\right)c^2\left(\frac{dt}{d\tau}\right)^2 + \left(1 - \frac{2GM}{c^2r}\right)^{-1}\left(\frac{dr}{d\tau}\right)^2 + r^2\left(\left(\frac{d\theta}{d\tau}\right)^2 + \sin^2(\theta)\left(\frac{d\varphi}{d\tau}\right)^2\right)\right] \end{aligned} \quad (4.4)$$

where τ denotes the proper time experienced by the particle.

The conserved quantities (4.3a) and (4.3b) are now identified as:

$$E = \left(1 - \frac{2GM}{c^2r}\right)c^2\frac{dt}{d\tau} = \text{constant}, \quad (4.5a)$$

$$L_z = r^2\sin^2(\theta)\frac{d\varphi}{d\tau} = \text{constant}, \quad (4.5b)$$

where the angular momentum referred to here is the component aligned with the BH's axis (the z-axis) [36]. On the other hand, we have²

$$|\vec{L}|^2 \equiv L^2 = \left(\frac{d\theta}{d\tau}\right)^2 r^4 + \frac{L_z^2}{\sin^2(\theta)} = \text{constant}, \quad (4.6)$$

¹ $\xi = \partial/\partial t$ and $\eta = \partial/\partial \varphi$

²Note that $\vec{L} = (L_x, L_y, L_z)$

where we distinguish between [36]

$$L_x = -r^2 \sin^2(\varphi) \frac{d\theta}{d\tau} - r^2 \cos^2(\varphi) \cos(\theta) \sin(\theta) \frac{d\varphi}{d\tau}, \quad (4.7a)$$

$$L_y = r^2 \cos^2(\varphi) \frac{d\theta}{d\tau} - r^2 \sin^2(\varphi) \cos(\theta) \sin(\theta) \frac{d\varphi}{d\tau}. \quad (4.7b)$$

The equations of motion (EoM) are then

$$\left(\frac{dt}{d\tau} \right)^2 = E^2 \left(\frac{2GM}{c^2 r} \right)^{-2} c^2 \Big|_{c=G=1} = E^2 \left(\frac{2M}{r} \right)^{-2} \Big|_{E=M=1, \theta=\frac{\pi}{2}} = \left(\frac{2}{r} \right)^{-2}, \quad (4.8a)$$

$$\left(\frac{dr}{d\tau} \right)^2 = E^2 - \frac{L^2}{r^2} \left(\frac{2GM}{c^2 r} \right) \Big|_{c=G=1} = E^2 - \frac{L^2}{r^2} \left(\frac{2M}{r} \right) \Big|_{E=M=1, \theta=\frac{\pi}{2}} = -\frac{L_z^2}{r^2} + \frac{2L_z^2}{r^3} + \frac{2}{r}, \quad (4.8b)$$

$$\left(\frac{d\theta}{d\tau} \right)^2 = \frac{L^2}{r^4} - \frac{L_z^2}{r^4 \sin^2(\theta)} \Big|_{c=G=1} = \frac{L^2}{r^4} - \frac{L_z^2}{r^4 \sin^2(\theta)} \Big|_{E=M=1, \theta=\frac{\pi}{2}} = 0, \quad (4.8c)$$

$$\left(\frac{d\varphi}{d\tau} \right)^2 = \frac{L_z^2}{r^4 \sin^4(\theta)} \Big|_{c=G=1} = \frac{L_z^2}{r^4 \sin^4(\theta)} \Big|_{E=M=1, \theta=\frac{\pi}{2}} = \frac{L_z^2}{r^4}. \quad (4.8d)$$

For simplicity, we will work in a system of geometrized units where both the speed of light (c) and the universal gravitational constant (G) are set to 1 [37] (see Appendix B). That's why we have simplified the EoM in addition to have considered that the mass of the BH (M) and the energy of the particle coming from infinity (E) are both 1, and that we are in the eq. plane³.

Adjusting terms (from here on, we rename L_z as ℓ)

$$\frac{dt}{d\tau} = \left(\frac{2}{r} \right)^{-1}, \quad (4.9a)$$

$$\frac{dr}{d\tau} = -\frac{1}{r^2} \sqrt{r(2r^2 + 2\ell^2 - r\ell^2)}, \quad (4.9b)$$

$$\frac{d\varphi}{d\tau} = \frac{\ell}{r^2}. \quad (4.9c)$$

Once the solutions to the geodesic equation are obtained, we can determine the squared COM energy of the collision (assuming equal masses ($m_1 = m_2 = m_0$))

$$E_{COM}^2 = 2m_1 m_2 \left(1 + \frac{(m_1 - m_2)^2}{2m_1 m_2} - g_{\mu\nu} u_{(1)}^\mu u_{(2)}^\nu \right) \Big|_{m_1=m_2=m_0} = 2m_0^2 \left(1 - g_{\mu\nu} u_{(1)}^\mu u_{(2)}^\nu \right), \quad (4.10)$$

where $u_{(1)}^\mu$ and $u_{(2)}^\nu$ represent the 4-velocities of the particles and the product

$$g_{\mu\nu} u_{(1)}^\mu u_{(2)}^\nu = g_{tt} u_{(1)}^t u_{(2)}^t + g_{rr} u_{(1)}^r u_{(2)}^r + g_{\varphi\varphi} u_{(1)}^\varphi u_{(2)}^\varphi. \quad (4.11)$$

If we combine this with (4.10), we obtain

$$(E_{COM}^{Schw})^2 = \frac{2m_0^2}{r^2(r-2)} \left[2r^2(r-1) - \ell_1 \ell_2 (r-2) - \sqrt{2r^2 - \ell_1^2(r-2)} \sqrt{2r^2 - \ell_2^2(r-2)} \right]. \quad (4.12)$$

Its analogous expression, without setting the BH mass to unity, is

$$(E_{COM}^{Schw})^2 = \frac{2m_0^2}{r^2(r-2M)} \left[2r^2(r-M) - \ell_1 \ell_2 (r-2M) - \sqrt{2Mr^2 - \ell_1^2(r-2M)} \sqrt{2Mr^2 - \ell_2^2(r-2M)} \right]. \quad (4.13)$$

³The eq. plane is restricted to $\theta = \pi/2$

Now, we are interested in bringing expression (4.12) to the horizon (located at $r = 2$) to study its behavior

$$\lim_{r \rightarrow 2} \left[\frac{2m_0^2}{r^2(r-2)} \left[2r^2(r-1) - \ell_1 \ell_2(r-2) - \sqrt{2r^2 - \ell_1^2(r-2)} \sqrt{2r^2 - \ell_2^2(r-2)} \right] \right] = \frac{0}{0}, \quad (4.14)$$

resulting in an indeterminate form of type $\frac{0}{0}$ (see Appendix C for the procedure). The **COM** energy finally becomes

$$E_{COM}^{Schw}(r \rightarrow 2) = \frac{m_0}{2} \sqrt{(l_2 - l_1)^2 + 16..} \quad (4.15)$$

This expression has a maximum when ℓ_1 and ℓ_2 are opposite ($\ell_1 = 4$ and $\ell_2 = -4$, and viceversa), meaning that we obtain:

$$E_{COM}^{Schw} = 2\sqrt{5}m_0. \quad (4.16)$$

On the other hand, if both are equal,

$$E_{COM}^{Schw} = 2m_0. \quad (4.17)$$

We can see that efficiently accelerating particles from **LEs** to ultra-**HES** is highly challenging, as it requires an extremely large number of collisions within a reasonable timeframe, making the process in this spacetime inefficient [32]. Before exploring other spacetimes, we will plot expressions (4.9b) and (4.12) to analyze this behavior in the Schwarzschild spacetime.

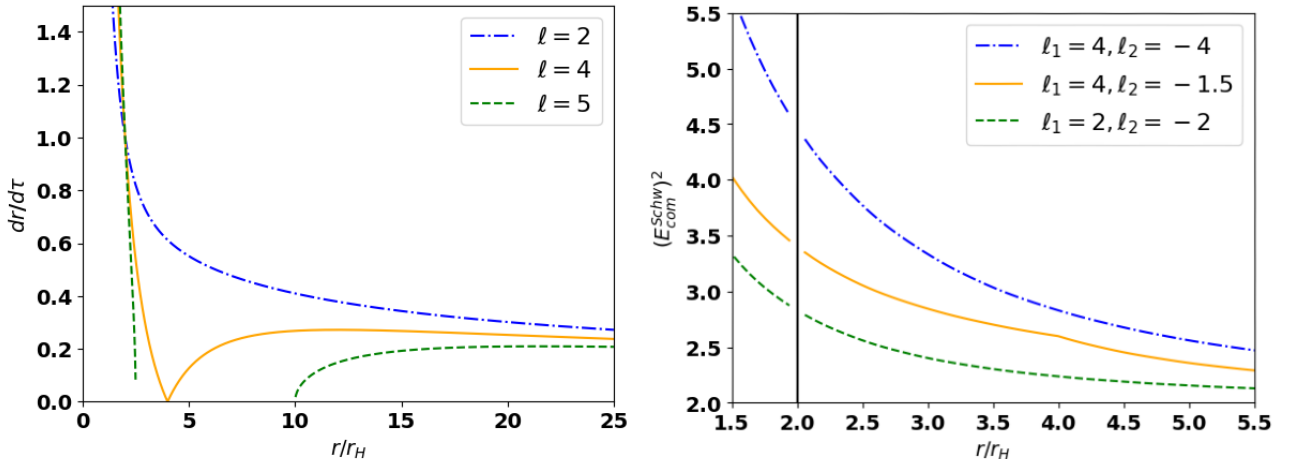


Figure 4.2: **Left:** shows how the particle's velocity varies as a function of its proximity to the **BH** and angular momentum (r_H represents the Schwarzschild horizon). **Right:** illustrates how the particle's squared **COM** energy changes as it approaches the event horizon. Reproduced from [33].

From the left panel of Figure 4.2 we can study the behavior of particles around a **BH** depending on their angular momentum, which determines how much they spin as they approach. If the angular momentum is too high ($\ell = 5$), the particles orbit far from the **BH** and never reach the horizon, preventing the study of the nearby region. Conversely, if the angular momentum is too low ($\ell = 2$), the particles fall almost straight into the **BH** with little lateral velocity, limiting the energy of their collisions. There is a critical angular momentum value ($\ell = 4$) where particles reach the horizon with the maximum possible lateral velocity, allowing for highly energetic collisions. [33].

On the other hand, the right panel depicts how the particle's **COM** energy varies with its proximity to the **BH** and different angular momentum values. Notable energy changes occur, especially in critical situations like $\ell = 4$. Near the event horizon, the energy remains finite, showing that it does not diverge [33].

4.2 Kerr black hole

Now, we dig into the context of rotating BHs, also known as Kerr BHs. We will perform an analogous treatment to the previous section, assuming the motion of particles on the eq. plane. We begin, this time, with the Kerr metric in Boyer-Lindquist coordinates [38].

$$ds^2 = -\frac{\Delta}{\rho^2} (dt - a \sin^2(\theta) d\varphi)^2 + \frac{\sin^2(\theta)}{\rho^2} [(r^2 + a^2) d\varphi - adt]^2 + \frac{\rho^2}{\Delta} dr^2 + \rho^2 d\theta^2, \quad (4.18)$$

where

$$\Delta \equiv r^2 + a^2 - 2GMr, \quad \rho^2 \equiv r^2 + a^2 \cos^2(\theta), \quad a \equiv \frac{J}{Mc}. \quad (4.19)$$

This last term is the Kerr parameter (a), composed of the angular momentum (J) and the mass (M) of the BH, respectively.

The Kerr metric in these coordinates is independent of the variables t and φ , and therefore, it is possible to obtain two constants of motion, just as in the Schwarzschild spacetime [39].

$$E = -\xi \cdot \vec{p} = -g_{\mu\nu}\xi^\mu p^\nu = -g_{t\nu}p^\nu = -p_t \quad (4.20a)$$

$$L_z = \eta \cdot \vec{p} = -g_{\mu\nu}\eta^\mu p^\nu = -g_{\varphi\nu}p^\nu = p_\varphi, \quad (4.20b)$$

After constructing the Lagrangian of a point particle, as in the Schwarzschild case, assuming the geometrized units system [37] and renaming L_z as ℓ , the geodesic solutions would be [40]

$$\rho^2 \frac{dr}{d\tau} = \pm \frac{1}{r^2} \sqrt{T^2 - \Delta(m_0^2 r^2 + (\ell - aE)^2)}, \quad (4.21a)$$

$$\rho^2 \frac{d\theta}{d\tau} = \pm \sqrt{Q - \cos^2(\theta) \left(a^2(m_0^2 - E^2) + \frac{\ell^2}{\sin^2(\theta)} \right)}, \quad (4.21b)$$

$$\rho^2 \frac{d\varphi}{d\tau} = - \left(aE - \frac{\ell}{\sin^2(\theta)} \right) + \frac{aT}{\Delta}, \quad (4.21c)$$

$$\rho^2 \frac{dt}{d\tau} = -a(aE \sin^2(\theta) - \ell) + (r^2 + a^2) \frac{T}{\Delta}. \quad (4.21d)$$

where we have defined T and Q (Carter constant) as

$$T = E(r^2 + a^2) - \ell a, \quad Q = p_\theta^2 + \cos^2(\theta) \left(a(m_0^2 - p_t^2) + \frac{p_\varphi^2}{\sin^2(\theta)} \right). \quad (4.22)$$

Once the geodesic EoM are calculated, we assume that the motion occurs in the eq. plane where $\rho^2 = r^2$ and the Carter constant vanishes. Therefore, the collection of geodesics will be

$$\frac{dr}{d\tau} = \pm \frac{1}{r^2} \sqrt{T^2 - \Delta(m_0^2 r^2 + (\ell - aE)^2)}, \quad (4.23a)$$

$$\frac{d\varphi}{d\tau} = -\frac{1}{r^2} \left[(aE - \ell) + a \frac{T}{\Delta} \right], \quad (4.23b)$$

$$\frac{d\varphi}{d\tau} = -\frac{1}{r^2} \left[a(aE - \ell) + (r^2 + a^2) \frac{T}{\Delta} \right]. \quad (4.23c)$$

The particle will approach the horizon from infinity, resulting in a defined range for the angular momentum of the particles (see Appendix D for the discussion)

$$-2 \left(1 + \sqrt{1 + \frac{a}{M}} \right) = \ell_L \leq \ell \leq \ell_R = 2 \left(1 + \sqrt{1 - \frac{a}{M}} \right). \quad (4.24)$$

This helps us confirm that the mechanism will only be possible for BHs with $a/M = 1$, which is equivalent to having an extremal BH ($a = M$) (see Figure D.1).

Finally, we can calculate the squared COM energy following the same steps as in the previous section. However, we will first assume that particles are *marginally bound*, resulting in

$$\begin{aligned} (E_{COM}^{Kerr})^2 = \frac{2m_0^2}{r(r^2 - 2Mr + a^2)} & (2a^2(r + M) - 2Ma(\ell_2 + \ell_1) - \ell_2\ell_1(r - 2M) + 2(r - M)r^2 \\ & - \sqrt{2M(a - \ell_2)^2 - \ell_2^2r + 2Mr^2}\sqrt{2M(a - \ell_1)^2 - \ell_1^2r + 2Mr^2}). \end{aligned} \quad (4.25)$$

If we bring this energy to the outer event horizon in an extremal Kerr BH, we obtain the COM energy

$$E_{COM}^{Kerr}(r \rightarrow r_+ = M) = \sqrt{2}m_0 \sqrt{\frac{\ell_2 - 2M}{\ell_1 - 2M} + \frac{\ell_1 - 2M}{\ell_2 - 2M}}. \quad (4.26)$$

The equation demonstrates that when ℓ_1 or ℓ_2 equals $2M$, the COM energy at the point of collision becomes unbounded, as shown in the right panel of Figure 4.3 [33].

So, there is a special situation where these particles have the maximum possible ℓ as they fall, and this happens when $\ell = 2M$. Usually, particles move towards the BH as if they were dropping straight down, causing them to collide gently because they are all moving in the same direction. However, in this special case, the particles do not fall straight but at an angle, like sliding to the side. This gives them lateral velocity, which means that when they collide, they do so with much more force and energy, creating far more intense collisions than if they were simply falling straight into the BH [33].

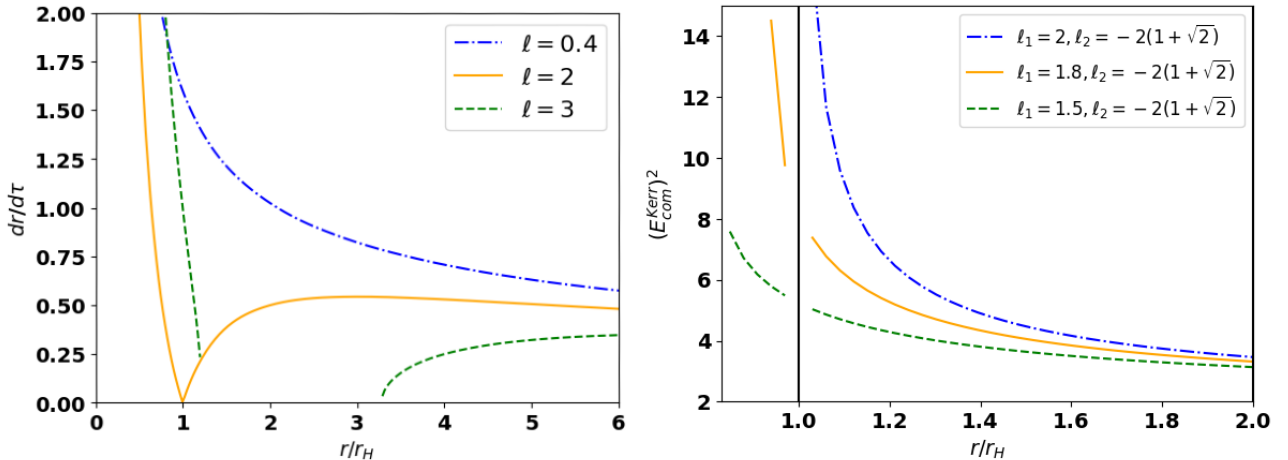


Figure 4.3: **Left:** illustrates how particle's velocity varies with radius for different angular momenta in an extremal Kerr BH (r_H represents the Schwarzschild horizon). **Right:** shows the squared COM energy variation with radius for three combinations of ℓ_1 and ℓ_2 . When $\ell_1 = 2$ (considering $M = 1$), the COM energy becomes infinite at the horizon [33].

Efficiency of the BSW mechanism

When studying this kind of processes, one must take a moment to examine the feasibility and efficiency of them. The original BSW mechanism [33] could be considered as a Penrose collisional process [41] in which the fact that the product particle escapes to infinity has not been taken into account. Therefore, in this section, we will consider particle collisions as in the BSW process, but this time with a product that escapes to infinity [42].

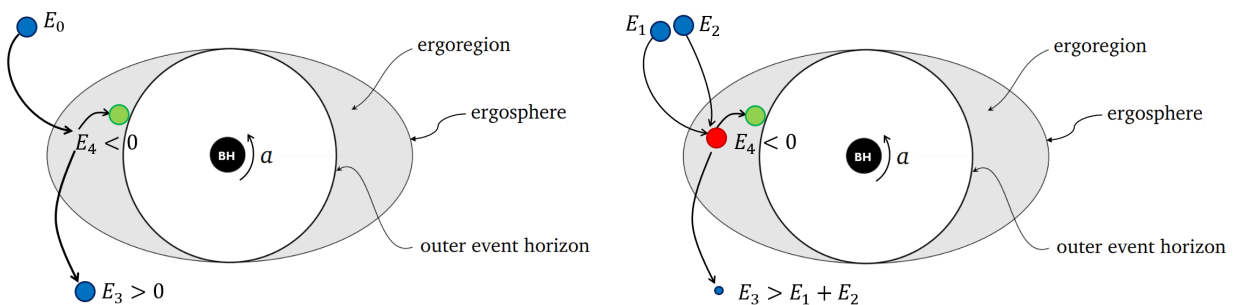


Figure 5.1: Energy extraction mechanisms near a rotating BH. **Left:** classic Penrose process [43], where a particle E_0 enters the ergosphere, splits, and one fragment $E_3 > E_0$ escapes while the other $E_4 < 0$ falls into the BH, extracting energy. **Right:** collisional Penrose process [41], where two incoming particles E_1 and E_2 collide within the ergosphere, producing an outgoing particle E_3 with energy greater than the sum of the incoming energies, also demonstrating energy extraction. Reproduced from [42].

Following the mathematical and physical treatment outlined in [42], we will calculate the energy of the third particle and the maximum efficiency achievable in different particle interactions (see Appendix E). This formula ends up to be (where we have redefined $\sin(\theta)$ as s_θ)

$$E_{3,r \rightarrow 1}(E_1, m_1, \tilde{p}_1^\theta, \tilde{p}_3^\theta, s_\theta) = \frac{2E_1 s_\theta + \epsilon_1 \sqrt{(m_1^2 - E_1^2)s_\theta^4 + (8E_1^2 - 2m_1^2 - E_1^2(\tilde{p}_1^\theta)^2)s_\theta^2 - 4E_1^2}}{2s_\theta - \sqrt{-s_\theta^4 + (8 - (\tilde{p}_3^\theta)^2)s_\theta^2 - 4}}. \quad (5.1)$$

5.1 Particle interactions

Throughout this section, we will seek the maximum optimization of equation (5.1) for different particle interactions. The reactions will be described by three letters representing the two reactants and the escaping product, with M representing any massive particle and P representing a

photon. These reactions will be accompanied by a symbol: (+) for the case where the critical particle (1) skirts the **BH**, or (–) when it goes directly from infinity towards the event horizon (what we previously defined as *outgoing* and *ingoing*).

5.1.1 Interactions with an escaping photon

This subsection is dedicated to the study of particle interactions in which the particle that escapes to infinity (3) is massless. The reactions we will study are: **MMP**, **PMP**, and **MPP**. We aim to optimize this equation to the fullest, so we will apply it to an **MMP-** collision located in the [eq. plane](#).

The procedure we will follow is applicable to the rest of the interactions. When we encounter a (–) case, the term \tilde{p}_1^θ causes the collisions to reach their maximum value when the particle flies with its maximum allowed polar momentum [42]. Meanwhile, for the (+) cases, the maximum energies are linked to a zero value of this function because we are considering processes in the [eq. plane](#). On the other hand, the equation for the maximum energy is optimized when the function \tilde{p}_3^θ equals zero, regardless of the case we are in [42].

We will also consider that the first and third particles are critical ($L_1 = b_1 E_1 = 2$ and $b_3 = 2$), while the second particle is subcritical ($b_2 < 2$). Additionally, we will assume that the mass of the massive particles is unity, whereas it will be zero for photons.

Starting with equation (5.1), we will substitute the initial data of the process ($E_1 = m_1 = 1$, $\epsilon_1 = -1$):

$$E_{3,r \rightarrow 1}(\tilde{p}_1^\theta, \tilde{p}_3^\theta, s_\theta) = \frac{2s_\theta - \sqrt{(6 - (\tilde{p}_1^\theta)^2)s_\theta^2 - 4}}{2s_\theta - \sqrt{-s_\theta^4 + (8 - (\tilde{p}_3^\theta)^2)s_\theta^2 - 4}}. \quad (5.2)$$

This energy will be fully optimized as long as

$$(\tilde{p}_1^\theta)^2 = \frac{6s_\theta^2 - 4}{s_\theta^2} \equiv (\tilde{p}_{1,\max}^\theta)^2(s_\theta), \quad (5.3)$$

which will cancel the square root. Then, taking this value along with $\tilde{p}_3^\theta = 0$ and assuming that this is happening in the [eq. plane](#), we have

$$E_{3,r \rightarrow 1}(s_\theta) = \left. \frac{2s_\theta}{2s_\theta - \sqrt{-s_\theta^4 + 8s_\theta^2 - 4}} \right|_{\theta=\pi/2} = \frac{2}{2 - \sqrt{3}} = 4 + 2\sqrt{3} \approx 7.46. \quad (5.4)$$

This will make the efficiency to be

$$\eta_{MMP-} = \frac{E_3}{E_1 + E_2} = \frac{4 + 2\sqrt{3}}{1 + 1} \approx 3.73. \quad (5.5)$$

The maximum energies and efficiencies of the other cases (MMP+, PMP-, PMP+, MPP- and MPP+) are calculated in Appendix F. Below it's possible to find a table with the results of all the reactions.

The PMP+ and MPP+ collisions exhibit the highest efficiencies, with maximum values of 13.92 and 12.74, respectively, suggesting that configurations where the critical particle skirts the **BH** are more favorable. In contrast, the MMP- collision has the lowest efficiency, reaching only 3.73, indicating that the configuration in which the critical particle heads directly towards the event horizon is the least efficient.

Table 5.1: Distribution of maximum energies and efficiencies obtained for the different particle interactions in which particle (3) is massless. (a) indicates that it was achieved when $E_1 \rightarrow \infty$. (b) indicates when $E_1 \rightarrow 0$. Reproduced from [42].

	Maximal energy	Maximal efficiency	Particle interaction
MMP-	$4 + 2\sqrt{3} \approx 7.46$	$2 + \sqrt{3} \approx 3.73$	(-) pair annihilation
MMP+	$(2 + \sqrt{2})/(2 - \sqrt{3}) \approx 12.74$	$(2 + \sqrt{2})/2(2 - \sqrt{3}) \approx 6.37$	(+) pair annihilation
PMP-	$2E_1/(2 - \sqrt{3}) \approx 7.46E_1$	$2(2 + \sqrt{3}) \approx 7.46^a$	(-) Compton scattering
PMP+	$(7 + 4\sqrt{3})E_1 \approx 13.92$	$(7 + 4\sqrt{3}) \approx 13.92^a$	(+) Compton scattering
MPP-	$4 + 2\sqrt{3} \approx 7.46$	$4 + 2\sqrt{3} \approx 7.46^b$	(-) ICS
MPP+	$(2 + \sqrt{2})/(2 - \sqrt{3}) \approx 12.74$	$(2 + \sqrt{2})/(2 - \sqrt{3}) \approx 12.74^b$	(+) ICS

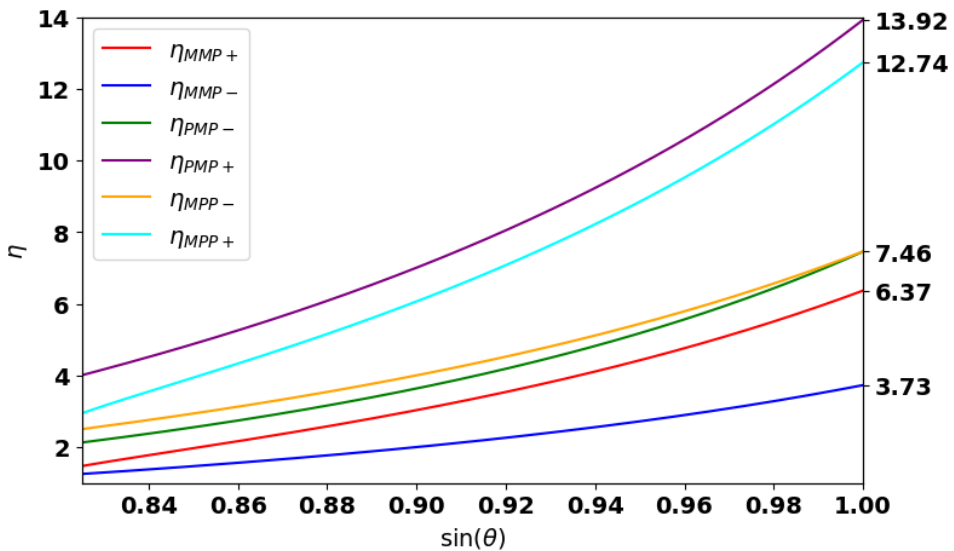


Figure 5.2: Efficiency (η) as a function of $\sin(\theta)$ for different particle collisions: MMP+, MMP-, PMP-, PMP+, MPP-, and MPP+. The curves show how the efficiency increases as $\sin(\theta)$ approaches 1, indicating that collisions in the equatorial plane are more efficient. The PMP+ and MPP+ cases exhibit the highest efficiencies, while MMP- shows the lowest. Reproduced from [42].

5.1.2 Interactions with an escaping massive particle

In this subsection, we will explore different cases where the particle escaping to infinity has a mass ($m_3 \neq 0$). Specifically, we will study the processes: MMM, PMM, and MPM. The analogous version of expression (5.2) for these processes is

$$E_{3,r \rightarrow 1}(E_1, m_1, \tilde{p}_1^\theta, s_\theta, \alpha_3) = \frac{2E_1 s_\theta + \epsilon_1 \sqrt{(m_1^2 - E_1^2)s_\theta^4 + (8E_1^2 - 2m_1^2 - E_1^2(\tilde{p}_1^\theta)^2)s_\theta^2 - 4E_1^2}}{2s_\theta - \sqrt{8s_\theta^2 - s_\theta^4 - 4 - \alpha_3^2(2s_\theta^2 - s_\theta^4)}}. \quad (5.6)$$

In the case of an MMM+ process ($E_1 = m_1 = \epsilon_1 = 1$ and $\tilde{p}_1^\theta = 0$)

$$E_{3,r \rightarrow 1}(s_\theta, \alpha_3) = \frac{2s_\theta + \sqrt{6s_\theta^2 - 4}}{2s_\theta - \sqrt{8s_\theta^2 - s_\theta^4 - 4 - \alpha_3^2(2s_\theta^2 - s_\theta^4)}}. \quad (5.7)$$

If we consider that the process occurs in the eq. plane

$$E_{3,r \rightarrow 1}(\alpha_3) = \frac{2 + \sqrt{6 - 4}}{2 - \sqrt{8 - 1 - 4 - \alpha_3^2(2 - 1)}} = \frac{2 + \sqrt{2}}{2 - \sqrt{3 - \alpha_3^2}} \Big|_{E_3=1/\alpha_3} \rightarrow \alpha_3 = \frac{7 - 4\sqrt{2}}{17}, \quad (5.8)$$

If we substitute it into (5.8), we obtain

$$E_{3,r \rightarrow 1} = \frac{2 + \sqrt{2}}{2 - \sqrt{3 - \left(\frac{7-4\sqrt{2}}{17}\right)^2}} = 7 + 4\sqrt{2} \approx 12.66. \quad (5.9)$$

Then, the maximum efficiency will be

$$\eta_{MMM+} = \frac{E_3}{E_1 + E_2} = \frac{7 + 4\sqrt{2}}{1 + 1} = \frac{7 + 4\sqrt{2}}{2} \approx 6.32. \quad (5.10)$$

The rest of the cases can be calculated in a similar way (see Appendix G) and are summarized in the following table:

Table 5.2: Distribution of maximum energies and efficiencies obtained for the different particle interactions in which particle (3) is massive. (a) indicates that it was achieved when $E_1 \rightarrow \infty$. (b) indicates when $E_1 \rightarrow 0$. Reproduced from [42].

	Maximal energy	Maximal efficiency	Particle interaction
MMM-	$4 + \sqrt{11} \approx 7.32$	$4 + \sqrt{11}/2 \approx 3.66$	(-) elastic scattering
MMM+	$7 + 4\sqrt{2} \approx 12.66$	$7 + 4\sqrt{2}/2 \approx 6.32$	(+) elastic scattering
PMM-	$4E_1 + \sqrt{(12E_1^2 - 1)}$	$4 + 2\sqrt{3} \approx 7.46^a$	(-) photomeson production
PMM+	$7.46E_1 + \sqrt{(41.78E_1^2 - 1)}$	$(4 + 2\sqrt{3}) + \sqrt{(3(7 + 4\sqrt{3}))} \approx 13.92^a$	(+) photomeson production
MPM-	$4 + \sqrt{11} \approx 7.32$	$4 + \sqrt{11} \approx 7.32^b$	(-) ICS
MPM+	$7 + 4\sqrt{2} \approx 12.66$	$7 + 4\sqrt{2} \approx 12.66^b$	(+) ICS

In Figure 5.3, we observe a graph similar to Figure 5.2, but for the case where the particle escaping to infinity is massive, all as a function of the angle. The configurations MPM+ and PMM+ reach the highest efficiencies, with maximum values of 13.92 and 12.66, respectively. On the other hand, the MMM- and MMM+ collisions exhibit the lowest efficiencies.

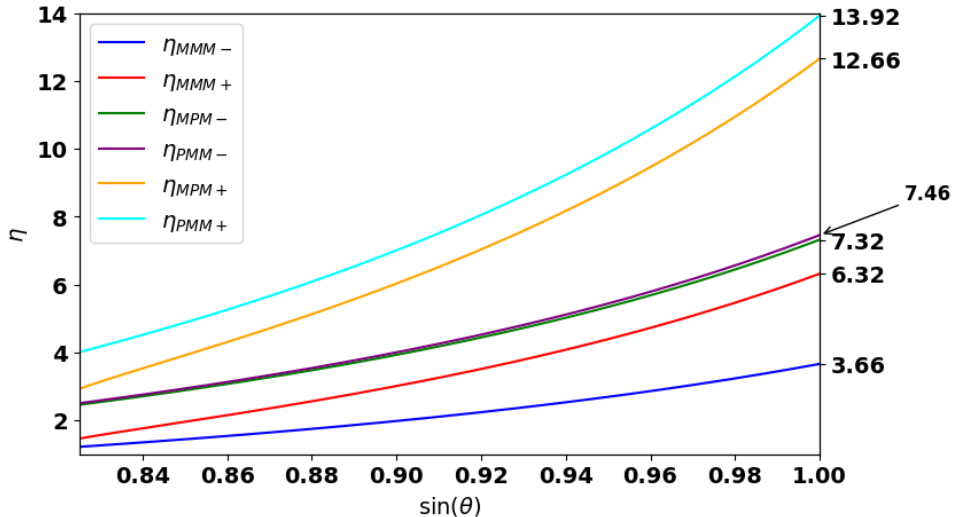


Figure 5.3: Efficiency (η) versus $\sin(\theta)$ for collisions between critical and subcritical particles in MMM+, MMM-, PMM-, PMM+, MPM-, and MPM+ processes. Efficiencies increase as they approach the equatorial plane, being highest in the PMM+ and MPM+ cases, and lowest in the MMM- and MMM+ configurations. Reproduced from [42].

Discussion

We have found the **COM** energy in two different spacetimes: Schwarzschild and Kerr. For the Schwarzschild black hole (BH), the energy is given by:

$$E_{COM}^{Schw}(r \rightarrow 2) = \frac{m_0}{2} \sqrt{(\ell_2 - \ell_1)^2 + 16}, \quad (6.1)$$

which reaches its maximum when $\ell_1 = 4$ and $\ell_2 = -4$, or vice versa, yielding a value of $2\sqrt{5}m_0$. This energy cannot be considered as **HE**, highlighting the limitations of the Bañados-Silk-West (BSW) effect in resolving the origin of ultra-high-energy cosmic rays (UHECRs) as it fails to reach the required extreme energies.

In this spacetime, we conclude that particles around a **BH** are strongly influenced by their angular momentum. Particles with high angular momentum ($\ell = 5$) remain in orbit far from the **BH**, while those with low angular momentum ($\ell = 2$) fall almost directly into the **BH**, limiting the collision energy. There is a critical angular momentum ($\ell = 4$) where particles reach the horizon with maximum lateral velocity, enabling highly energetic collisions. Notably, the **COM** energy remains finite near the horizon, demonstrating that it does not diverge.

On the other hand, in Kerr spacetime, the **COM** energy found is:

$$E_{COM}^{Kerr}(r \rightarrow r_+ = M) = \sqrt{2}m_0 \sqrt{\frac{\ell_2 - 2M}{\ell_1 - 2M} + \frac{\ell_1 - 2M}{\ell_2 - 2M}}, \quad (6.2)$$

which diverges and becomes unbounded when either ℓ_1 or ℓ_2 equals $2M$. This scenario represents a unique configuration where particles fall with the maximum possible angular momentum, allowing for collisions at extremely **HES** near the event horizon of extremal Kerr **BHs**.

Through the study of the effective potential, we have verified that the mechanism is only possible under a set of conditions:

- The angular momentum of one of the particles must be $\ell = 2M$.
- The Kerr black hole must be extremal ($a = M$).
- The angular momentum range found for the particles must be respected.

From our study of efficiency, we can confirm that the calculated values of E_3 and η were determined under the assumption of an extremal Kerr **BH**, as concluded earlier. We also considered that at least one of the particles had a critical impact parameter of $b = 2$, corresponding to the critical value found when analyzing the **BSW** effect in Kerr spacetime ($\ell = 2M$). These particles

have a turning point at the event horizon, which aligns with a jump observed in the Kerr plot precisely at the same point [42].

Furthermore, we noted that although the **COM** energy in this mechanism can become arbitrarily high and divergent, the outgoing particle energies (3) do not reach such extreme values [42]. For instance, if we compare the processes by differentiating them based on their products, we observe that when the escaping particle is a photon, the **COM** energy is higher, and therefore the efficiency is greater than when any other massive particle escapes. For example, the *ingoing* pair annihilation has a **COM** energy of 7.46 (this energy should be multiplied by the mass of particle (1) to obtain the actual value in a real case), while the *ingoing* elastic scattering has an energy of 7.32.

On the other hand, if we consider the kinematic nature of the particle (*ingoing* or *outgoing*), we can observe that all interactions accompanied by the symbol (+) have higher energies and efficiencies compared to their counterparts (−). This leads us to conclude that when one of the incoming particles orbits around the **BH**, it results in a more energetic reaction.

Although the **BSW** effect shows potential for particle collisions at arbitrarily **HEs**, these energies are not necessarily observable as outgoing particles do not retain such extreme energy levels. This effect could nonetheless provide an alternative probe for **DM** detection, as indicated in [34], since near **BHs**, the gravitational attraction significantly increases the density of **DM**, which intensifies particle collisions and enhances the emission of annihilation signals. This makes these environments ideal for exploring **DM** interactions. Even when particles approach near-light speeds, their collision energy remains limited, influencing the effectiveness of annihilation channels and potentially causing resonances that can impact the annihilation outcomes.

Furthermore, each particle interaction may initiate a cascade of subsequent reactions, progressively accumulating energy with each interaction step. For example, in **ICS**, $e^\pm + \gamma_{bg} \rightarrow e^\pm + \gamma$, each electron produced could interact with another photon, successively gaining energy (ΔE): the first electron, which would have an energy of 7.32 m_1 , would interact with another photon, resulting in an electron with an energy of $(\Delta E)^2$, and so on $(\Delta E)^n$, continuing this process until reaching very **HEs**.

In a **MM** context, photomeson production can lead to the creation of protons and neutral pions or neutrons and charged pions

$${}^A_Z X + \gamma_{bg} \rightarrow \Delta^+ \rightarrow \begin{cases} p + \pi^0, \\ n + \pi^+. \end{cases} \quad (6.3)$$

which in turn can trigger additional interactions,

$$\pi^0 \rightarrow \gamma + \gamma, \quad \pi^+ \rightarrow \mu^+ + \nu_\mu, \quad \mu^+ \rightarrow e^+ + \bar{\nu}_\mu + \nu_e. \quad (6.4)$$

generating new particles and messengers, thereby enhancing the overall energy output. These complex cascades underscore the intricate nature of **HE** environments near **BHs** and their role in astrophysical particle acceleration processes.

Thus, while the **BSW** mechanism probably won't solve the mystery of **UHECRs** origin due to energy constraints, it opens up avenues for detecting **HE** phenomena and probing the extreme physical conditions surrounding any kind of **BH**, potentially uncovering new insights into the nature of **DM** and **HE** astrophysical processes.

Summary

In this work, we explored the **COM** energy for particle collisions in two distinct spacetimes: Schwarzschild and Kerr. For the Schwarzschild **BH**, the **COM** energy reaches a finite maximum of $2\sqrt{5}m_0$ at critical angular momentum values, where m_0 is the mass of the incoming particles. This indicates that the scenario is not an efficient way to produce **UHECRs**, as it would require an extremely large number of collisions to raise a **LECR** to ultra-**HES**, which is highly unlikely within a reasonable timeframe given the limited number of **CRs**.

In contrast, our analysis also confirmed that the occurrence of these extreme energy collisions in Kerr spacetime is highly conditional, depending on the specific angular momentum of the particles and the extremality of the **BH**. Despite the potential for arbitrarily high **COM** energy, the actual energy of outgoing particles remains bounded and does not achieve such extreme levels. This suggests that the **BSW** effect, while capable of generating **HE** interactions, does not fully resolve the origin of **UHECRs**, as the observable energies are insufficient. In future work, we will perform calculations outside the **eq. plane** and explore these phenomena in greater depth.

We thought how the **BSW** effect could serve as an alternative method for detecting **DM** near **BHs**. The increased density of **DM** in the vicinity of **BHs** enhances particle interactions, potentially leading to distinctive annihilation signals. Even though the energy of individual collisions is limited, the cascading nature of successive interactions allows particles to accumulate energy progressively. These cascading processes underscore the complex and dynamic nature of **HE** environments near **BHs**, contributing to astrophysical particle acceleration and the generation of observable **HE** phenomena.

The findings of this study point to several avenues for future research. A deeper investigation into the exact conditions that allow for the most energetic interactions in Kerr spacetime could provide further insights into the limitations and potential of the **BSW** mechanism. Additionally, observational studies focused on detecting unique annihilation signals near **BHs** could help verify the theoretical predictions and potentially uncover new information about **DM**. Expanding the study to include other astrophysical scenarios, such as rotating neutron stars or alternative **BH** metrics (such as Reissner-Nordström or Kerr-Newman), could also broaden our understanding of **HE** processes in extreme gravitational fields. Finally, we are already performing numerical simulations with observational data using *CRPropa*¹, which is essential to validate the theoretical models and explore the practical implications of these **HE** cascades in real astrophysical environments.

¹CRPropa is a simulation tool used to model the propagation and interactions of **UHECRs** and associated particles in space [44, 45].

Bibliography

- [1] Maurizio Spurio. *Probes of Multimessenger Astrophysics: Charged cosmic rays, neutrinos, γ -rays and gravitational waves*. Astronomy and Astrophysics Library. Springer, 2018.
- [2] A. et al. Addazi. Quantum gravity phenomenology at the dawn of the multi-messenger era—a review. *Progress in Particle and Nuclear Physics*, 125:103948, July 2022.
- [3] Nataly Ospina. Multi-messenger astrophysics, Feb 2024.
- [4] Rafael Alves Batista. *Astrophysics with ultra-high-energy cosmic messengers*. 2023.
- [5] G. Breit and John A. Wheeler. Collision of two light quanta. *Phys. Rev.*, 46:1087–1091, Dec 1934.
- [6] Arthur H. Compton. A quantum theory of the scattering of x-rays by light elements. *Phys. Rev.*, 21:483–502, May 1923.
- [7] Rafael Alves Batista and Andrey Saveliev. The gamma-ray window to intergalactic magnetism. *Universe*, 7(7):223, July 2021.
- [8] Imre Bartos and Marek Kowalski. *Multimessenger Astronomy*. 2399-2891. IOP Publishing, 2017.
- [9] George R. Blumenthal. Energy loss of high-energy cosmic rays in pair-producing collisions with ambient photons. *Phys. Rev. D*, 1:1596–1602, Mar 1970.
- [10] Rafael Alves Batista. Computational methods for astroparticle propagation, 2023.
- [11] V. Berezinsky, A.Z. Gazizov, and S.I. Grigorieva. Dip in uhecr spectrum as signature of proton interaction with cmb. *Physics Letters B*, 612(3–4):147–153, April 2005.
- [12] Rafael Alves Batista. *Propagation of Astroparticles: a multimessenger view*. 2021.
- [13] Rafael Alves Batista, Jonathan Biteau, and Bustamante et al. Open questions in cosmic-ray research at ultrahigh energies. *Frontiers in Astronomy and Space Sciences*, 6, June 2019.
- [14] Kenneth Greisen. End to the cosmic-ray spectrum? *Phys. Rev. Lett.*, 16:748–750, Apr 1966.
- [15] G. T. Zatsepin and V. A. Kuz'min. Upper Limit of the Spectrum of Cosmic Rays. *Soviet Journal of Experimental and Theoretical Physics Letters*, 4:78, August 1966.

- [16] F. W. Stecker and M. H. Salamon. Photodisintegration of ultra-high-energy cosmic rays: A new determination. *The Astrophysical Journal*, 512(2):521–526, February 1999.
- [17] Sangjin Lee. Propagation of extragalactic high energy cosmic and rays. *Physical Review D*, 58(4), July 1998.
- [18] R. W. Brown, W. F. Hunt, K. O. Mikaelian, and I. J. Muzinich. Role of $\gamma + \gamma \rightarrow e^+ + e^- + e^+ + e^-$ in photoproduction, colliding beams, and cosmic photon absorption. *Phys. Rev. D*, 8:3083–3102, Nov 1973.
- [19] A. Borsellino. Sulle coppie di elettroni create da raggi in presenza di elettroni. *Il Nuovo Cimento*, 4(3–4):112–130, Jun 1947.
- [20] A. Friedman. On the curvature of space. *General Relativity and Gravitation*, 31(12):1991–2000, 1999.
- [21] Planck Collaboration. Planck2018 results: Vi. cosmological parameters. *Astronomy amp; Astrophysics*, 641:A6, September 2020.
- [22] M. Bustamante. High-energy cosmic-ray acceleration. In *2009 CERN-Latin-American School of High-Energy Physics, CLASHEP 2009 - Proceedings*, 2009 CERN-Latin-American School of High-Energy Physics, CLASHEP 2009 - Proceedings, pages 533–539. CERN, 2010. 2009 5th CERN-Latin-American School of High-Energy Physics, CLASHEP 2009 ; Conference date: 15-03-2009 Through 28-03-2009.
- [23] Hang Bae Kim. How can we find the sources of uhecr? *Journal of the Korean Physical Society*, 57(3(1)):655–659, Sep 2010.
- [24] Kseniya V Ptitsyna and Sergei V Troitsky. Physical conditions in potential accelerators of ultra-high-energy cosmic rays: updated hillas plot and radiation-loss constraints. *Physics-Uspekhi*, 53(7):691, oct 2010.
- [25] A. M. Hillas. The origin of ultra-high-energy cosmic rays. *Annual Review of Astronomy and Astrophysics*, 22(1):425–444, 1984.
- [26] ENRICO Fermi. On the origin of the cosmic radiation. *Phys. Rev.*, 75:1169–1174, Apr 1949.
- [27] R. J. Protheroe. Acceleration and interaction of ultra high energy cosmic rays, 1998.
- [28] Malcolm S. Longair. *High Energy Astrophysics*. 2011.
- [29] Rafael Alves Batista. *On the cosmological propagation of high energy particles in magnetic fields*. PhD thesis, U. Hamburg, Dept. Phys., 2015.
- [30] Tobias Winchen and Stijn Buitink. Energy spectrum of fast second order fermi accelerators as sources of ultra-high-energy cosmic rays. *Astroparticle Physics*, 102:25–31, November 2018.
- [31] W. I. Axford, E. Leer, and G. Skadron. The Acceleration of Cosmic Rays by Shock Waves. In *International Cosmic Ray Conference*, volume 11 of *International Cosmic Ray Conference*, page 132, January 1977.
- [32] Tomohiro Harada and Masashi Kimura. Black holes as particle accelerators: a brief review. *Classical and Quantum Gravity*, 31(24):243001, November 2014.

- [33] Máximo Bañados, Joseph Silk, and Stephen M. West. Kerr black holes as particle accelerators to arbitrarily high energy. *Physical Review Letters*, 103(11), September 2009.
- [34] ANTON BAUSHEV. Dark matter annihilation in the gravitational field of a black hole. *International Journal of Modern Physics D*, 18(08):1195–1203, August 2009.
- [35] Éric Gourgoulhon. Lecture notes - geometry and physics of black holes, 2024.
- [36] Eva Hackmann, Betti Hartmann, Claus Lämmerzahl, and Parinya Sirimachan. Complete set of solutions of the geodesic equation in the space-time of a schwarzschild black hole pierced by a cosmic string. *Physical Review D*, 81(6), March 2010.
- [37] Alan L. Myers. *NATURAL SYSTEM OF UNITS IN GENERAL RELATIVITY*.
- [38] Robert H. Boyer and Richard W. Lindquist. Maximal Analytic Extension of the Kerr Metric. *Journal of Mathematical Physics*, 8(2):265–281, February 1967.
- [39] Adam Cieślik, Eva Hackmann, and Patryk Mach. Kerr geodesics in terms of weierstrass elliptic functions. *Physical Review D*, 108(2), July 2023.
- [40] James M. Bardeen, William H. Press, and Saul A. Teukolsky. Rotating Black Holes: Locally Nonrotating Frames, Energy Extraction, and Scalar Synchrotron Radiation. , 178:347–370, December 1972.
- [41] T. Piran, J. Shaham, and J. Katz. High Efficiency of the Penrose Mechanism for Particle Collisions. , 196:L107, March 1975.
- [42] Elly Leiderschneider and Tsvi Piran. Maximal efficiency of the collisional penrose process. *Physical Review D*, 93(4), February 2016.
- [43] Roger Penrose. Gravitational Collapse: the Role of General Relativity. *Nuovo Cimento Rivista Serie*, 1:252, January 1969.
- [44] Rafael Alves Batista, Andrej Dundovic, and Martin et al. Erdmann. Crpropa 3—a public astrophysical simulation framework for propagating extraterrestrial ultra-high energy particles. *Journal of Cosmology and Astroparticle Physics*, 2016(05):038–038, May 2016.
- [45] Rafael Alves Batista, Julia Becker Tjus, and Julien et al. Dörner. Crpropa 3.2 — an advanced framework for high-energy particle propagation in extragalactic and galactic spaces. *Journal of Cosmology and Astroparticle Physics*, 2022(09):035, September 2022.
- [46] A. Domínguez, J. R. Primack, and D. J. et al. Rosario. Extragalactic background light inferred from aegis galaxy-sed-type fractions: Ebl from aegis galaxy-sed-type fractions. *Monthly Notices of the Royal Astronomical Society*, 410(4):2556–2578, October 2010.
- [47] Rudy C. Gilmore, Rachel S. Somerville, Joel R. Primack, and Alberto Domínguez. Semi-analytic modelling of the extragalactic background light and consequences for extragalactic gamma-ray spectra: Modelling of the ebl and gamma-ray spectra. *Monthly Notices of the Royal Astronomical Society*, 422(4):3189–3207, April 2012.
- [48] Floyd W. Stecker, Sean T. Scully, and Matthew A. Malkan. An empirical determination of the intergalactic background light from uv to fir wavelengths using fir deep galaxy surveys and the gamma-ray opacity of the universe. *The Astrophysical Journal*, 827(1):6, August 2016.
- [49] Wikipedia. Geometrized unit system, July 2024.

- [50] Guillaume-François-Antoine de (1661-1704). Auteur du texte L'Hospital. Analyse des infiniment petits, pour l'intelligence des lignes courbes . par mr le marquis de l'hospital. seconde édition, Jan 1970.
- [51] Tomohiro Harada and Masashi Kimura. Collision of two general geodesic particles around a kerr black hole. *Physical Review D*, 83(8), April 2011.
- [52] Michał Bejger, Tsvi Piran, Marek Abramowicz, and Frida Håkanson. Collisional penrose process near the horizon of extreme kerr black holes. *Physical Review Letters*, 109(12), sep 2012.

Energy losses of different particle interactions

Figure A.1 shows the attenuation lengths (λ) for various CR nuclei as a function of energy (E) [2]. It highlights how different energy loss mechanisms impact CRs based on type and energy. Photopion production, significant at higher energies, affects protons most, generating pions when CRs collide with CMB photons. Pair production, occurring at lower energies, affects all CRs by creating electron-positron pairs. Photodisintegration mainly impacts heavier nuclei like helium, nitrogen, and iron, breaking them into lighter particles upon interaction with CMB photons. Adiabatic losses, due to the Universe's expansion, affect all particles regardless of energy.

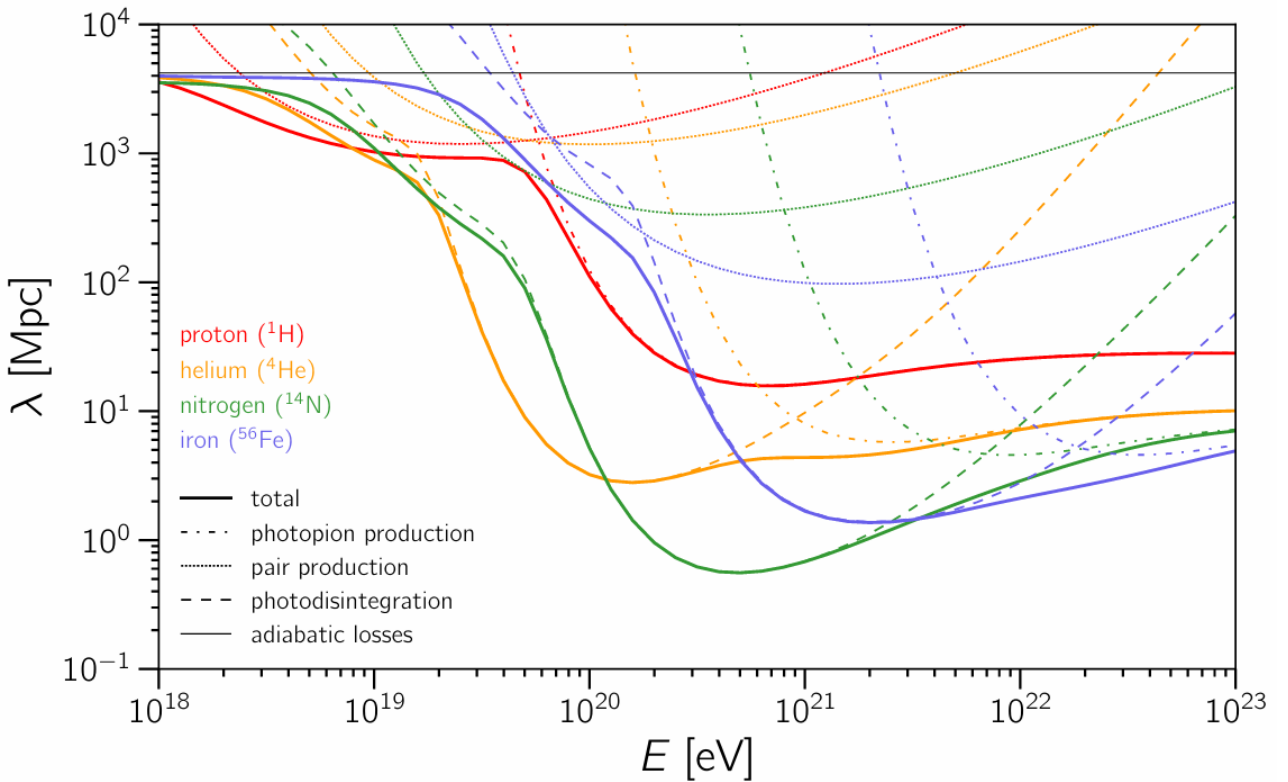


Figure A.1: Distribution of the attenuation length (λ) of different CR nuclei as a function of energy (E), illustrating how photopion production, pair production, photodisintegration, and adiabatic losses affect their travel distance. The attenuation length, measured in megaparsecs (Mpc), represents the average distance these CRs can travel before losing energy through interactions with the CMB and other processes [2].

The Figure A.2 show the interaction rates or the inverse of the mean free path for HE particles undergoing different processes: pair production, double pair production, ICS, and triplet pair production. The interaction rates are plotted against particle energy for various background photon fields, including the CMB, several models of the Extragalactic Background Light and the Cosmic Radio Background. Each model [46, 47, 48], reflects different assumptions about the photon field densities, significantly affecting the interaction rates, particularly at higher energies, where differences between models become more pronounced [7].

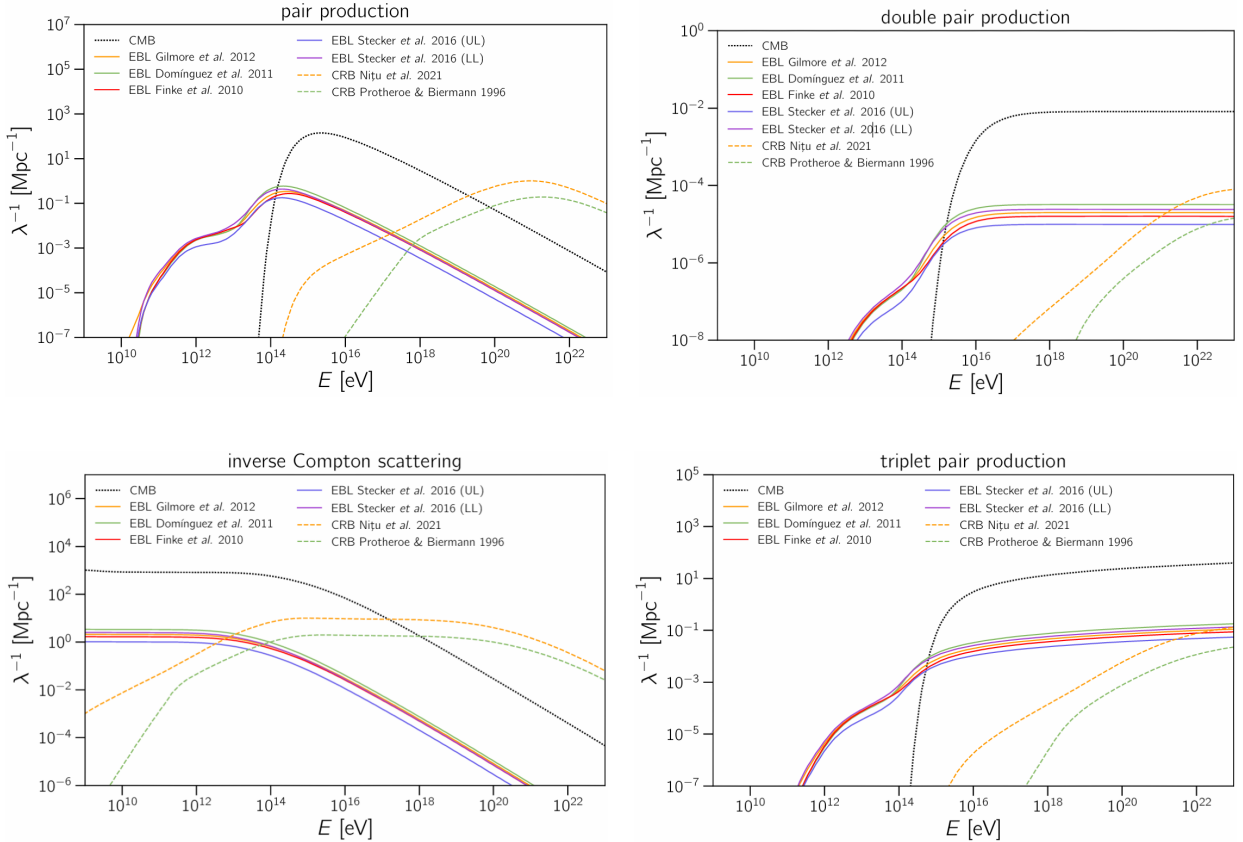


Figure A.2: Interaction rates (λ^{-1}) for various processes as a function of energy (E) for different models of background photon fields. The plots include pair production, double pair production, ICS, and triplet pair production [7].



Geometrized unit system

In this appendix, we provide a summary of the geometric units system introduced in [37].

A system of geometric units is one in which the speed of light (c) and the gravitational constant (G) are set equal to one:

$$c = G = 1. \quad (\text{B.1})$$

These constants are defined as:

$$c = 2.9979 \cdot 10^8 \left[\frac{m}{s} \right], \quad G = 6.66743 \cdot 10^{-11} \left[\frac{m^3}{kg \cdot s^{-2}} \right]. \quad (\text{B.2})$$

Since in this unit system the speed of light is considered as the unit, the time it takes light to travel a certain distance is the same as that distance, meaning that light is measured in units of length. Additionally, momentum and energy are components of the four-momentum, where mass represents its magnitude. Therefore, in geometric units, energy, momentum, and mass all share the dimensional unit of length [49].

In the context of the International System (IS) $[kg^\alpha \cdot m^\beta \cdot s^\gamma]$ and geometric units $[m^\alpha \cdot m^\beta \cdot m^\gamma]$, if we want to convert from the latter to the former, we multiply by

$$G^{-\alpha} \cdot c^{2\alpha-\gamma}. \quad (\text{B.3})$$

For example, the COM energy that we calculate multiple times throughout this document can be converted to the IS units as follows. The units of energy in the IS are $[kg \cdot m^2 \cdot s^{-2}]$, where we can identify $\alpha = 1$, $\beta = 2$, and $\gamma = -2$. Therefore, in geometric units, we have:

$$[kg \cdot m^2 \cdot s^{-2}] = [m^1 \cdot m^2 \cdot m^{-2}] = [m]. \quad (\text{B.4})$$

We can also find the conversion factor using (B.3):

$$G^{-\alpha} \cdot c^{2\alpha-\gamma} \Big|_{\alpha=1, \beta=2, \gamma=-2} = G^{-1} \cdot c^{2 \cdot 1 - (-2)} = G^{-1} \cdot c^4. \quad (\text{B.5})$$

Thus:

$$(1 \text{ m}) \left(\frac{c^4}{G^1} \right) = (1 \text{ m}) \frac{\left(2.9979 \cdot 10^8 \left[\frac{m}{s} \right] \right)^4}{6.66743 \cdot 10^{-11} \left[\frac{m^3}{kg \cdot s^{-2}} \right]} = 1.2102 \cdot 10^{44} [kg \cdot m^2 \cdot s^{-2}]. \quad (\text{B.6})$$

C

Resolution of expression (4.12) at the event horizon

In this appendix, the resolution of the indeterminacy arising in expression (4.14) is carried out after taking expression (4.12) to the event horizon (located at $r = 2$).

$$\lim_{r \rightarrow 2} \left[\frac{2m_0^2}{r^2(r-2)} \left[2r^2(r-1) - \ell_1 \ell_2(r-2) - \sqrt{2r^2 - \ell_1^2(r-2)} \sqrt{2r^2 - \ell_2^2(r-2)} \right] \right] = \frac{0}{0}, \quad (\text{C.1})$$

resulting in an indeterminate form of type $\frac{0}{0}$. Therefore, we apply L'Hôpital's rule [50], which states that:

$$\lim_{r \rightarrow a} \frac{f(r)}{g(r)} = \lim_{r \rightarrow a} \frac{f'(r)}{g'(r)}, \quad (\text{C.2})$$

if

- 1. $\lim_{r \rightarrow a} f(r) = \lim_{r \rightarrow a} g(r) = 0 \text{ or } \infty,$
- 2. $g'(r) \neq 0,$
- 3. $\exists \lim_{r \rightarrow a} \frac{f'(r)}{g'(r)}$ where $a \in \{\mathbb{R}, -\infty, +\infty\}.$

Let's verify the conditions:

$$\lim_{r \rightarrow 2} f(r) = \lim_{r \rightarrow 2} \left(2r^2(r-1) - \ell_1 \ell_2(r-2) - \sqrt{2r^2 - \ell_1^2(r-2)} \sqrt{2r^2 - \ell_2^2(r-2)} \right) = 0, \quad (\text{C.3a})$$

$$\lim_{r \rightarrow 2} g(r) = \lim_{r \rightarrow 2} (r-2) = 0. \quad (\text{C.3b})$$

First, we have the limit of a product, so

$$\lim_{r \rightarrow 2} (\text{original}) = \lim_{r \rightarrow 2} \frac{1}{r^2} \cdot \lim_{r \rightarrow 2} \frac{f(r)}{g(r)}. \quad (\text{C.4})$$

We continue by calculating the derivatives of the numerator and denominator:

$$f'(r) = -\frac{(4r - \ell_1^2)\sqrt{2r^2 - \ell_2^2(r-2)}}{2\sqrt{2r^2 - \ell_1^2(r-2)}} - \frac{(4r - \ell_2^2)\sqrt{2r^2 - \ell_1^2(r-2)}}{2\sqrt{2r^2 - \ell_2^2(r-2)}} + 2r^2 + 4r(r-1) - \ell_1 \ell_2, \quad (\text{C.5a})$$

$$g'(r) = 1. \quad (\text{C.5b})$$

Then,

$$\frac{1}{4} \lim_{r \rightarrow 2} f'(r) = \frac{1}{4} \left(-\frac{(8-\ell_1^2)\sqrt{8}}{2\sqrt{8}} - \frac{(8-\ell_2^2)\sqrt{8}}{2\sqrt{8}} + 16 - \ell_1 \ell_2 \right) = \frac{(\ell_1 - \ell_2)^2 + 16}{8}. \quad (\text{C.6})$$

Reorganizing terms, we have

$$\frac{(E_{cm}^{Schw})^2}{2m_0^2} = \frac{(\ell_1 - \ell_2)^2 + 16}{8} \rightarrow (E_{cm}^{Schw})^2 = 2m_0^2 \frac{(\ell_1 - \ell_2)^2 + 16}{8} = \frac{m_0^2 ((\ell_1 - \ell_2)^2 + 16)}{4}, \quad (\text{C.7})$$

that finally becomes

$$E_{COM}^{Schw}(r \rightarrow 2) = \frac{m_0}{2} \sqrt{(\ell_2 - \ell_1)^2 + 16}. \quad (\text{C.8})$$



Angular momentum range for the BSW process in Kerr spacetime

One of the properties that can be observed in this spacetime is that from expression (4.23a), we can derive [51]

$$\frac{1}{2} \left(\frac{dr}{d\tau} \right)^2 + \frac{r^4}{\rho^4} V_{\text{eff}}(r) = 0, \quad (\text{D.1})$$

where the effective potential is defined as

$$V_{\text{eff}}(r) = -\frac{T^2 - \Delta [m_0^2 r^2 + (\ell - aE)^2]}{2r^4} - \frac{m_0^2 M}{r} + \frac{\ell^2 - a^2(E^2 - m_0^2)}{2r^2} - \frac{M(\ell - aE)^2}{r^3} - \frac{E^2 - m_0^2}{2} \quad (\text{D.2})$$

which, for *marginally bound* particles ($E^2 = m_0^2$) [51], behaves as

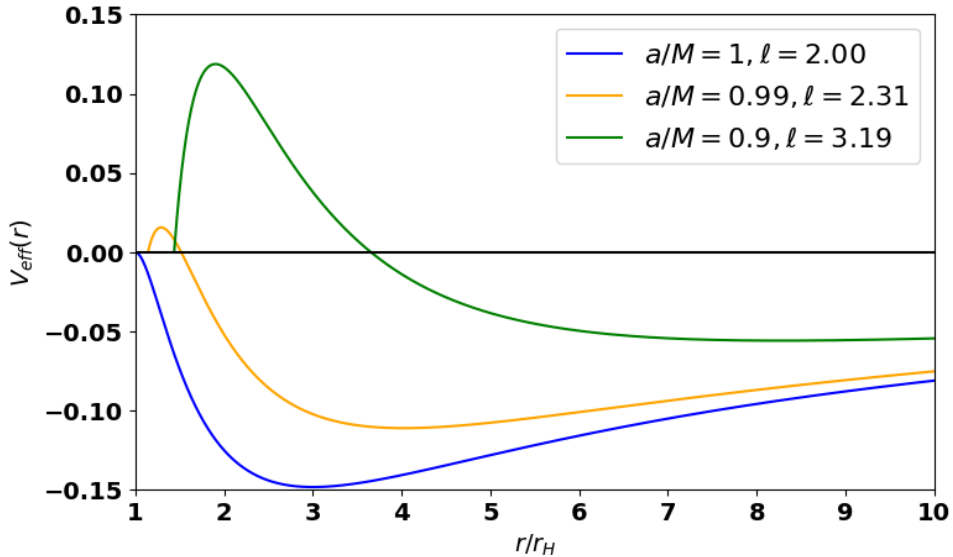


Figure D.1: Effective potential versus radius for marginally bound critical particles near a Kerr BH with varying spin parameters and angular momentum. The potential must remain non-positive in the allowed region of particle motion, indicating the stable and unstable orbits depending on the combination of a and ℓ . Reproduced from [32].

The event horizon in Kerr spacetime is located at

$$\Delta|_{G=1} = r^2 + a^2 - 2Mr \rightarrow \Delta = r^2 + a^2 - 2Mr = 0 \begin{cases} r_+ = M + \sqrt{M^2 - a^2} & \text{(outer event horizon),} \\ r_- = M - \sqrt{M^2 - a^2} & \text{(inner event horizon)} \end{cases} \quad (\text{D.3})$$

Then, the potential at the horizon becomes (see [32] for the mathematical treatment)

$$V_{\text{eff}}(r_+) = -\frac{(r_+^2 + a^2)^2 (m_0 - \Omega_{r_+} \ell)^2}{2r_+^4} \leq 0, \quad (\text{D.4})$$

where Ω_{r_+} is a constant derived from the calculation of the Killing horizons in Kerr spacetime (see section 10.5 in [35]). Now, if the effective potential is negative outside the horizon, we have the expression

$$2r^2 - M\ell^2 r + 2M^2 \left(\ell - \frac{a}{M} \right)^2 = 0. \quad (\text{D.5})$$

The particle will approach the horizon from infinity, resulting in a defined range for the angular momentum of the particles

$$-2 \left(1 + \sqrt{1 + \frac{a}{M}} \right) = \ell_L \leq \ell \leq \ell_R = 2 \left(1 + \sqrt{1 - \frac{a}{M}} \right). \quad (\text{D.6})$$

E

Mathematical treatment for the efficiency of the BSW mechanism

First of all, we will continue using a system of geometrized units [37]. The radial component of the momentum in Kerr spacetime is defined as

$$p^r = \epsilon \frac{\sqrt{V(r)}}{\rho^2}, \quad \text{with} \quad V(r) = (Er^2)^2 + (Era)^2 - r\ell^2(r - 2M) - 4MER\ell a + 2Mr(Ea)^2. \quad (\text{E.1})$$

The only unknown so far is ϵ , which can take the values ± 1 (negative when the particle is *ingoing*¹ and positive when the particle is *outgoing*²).

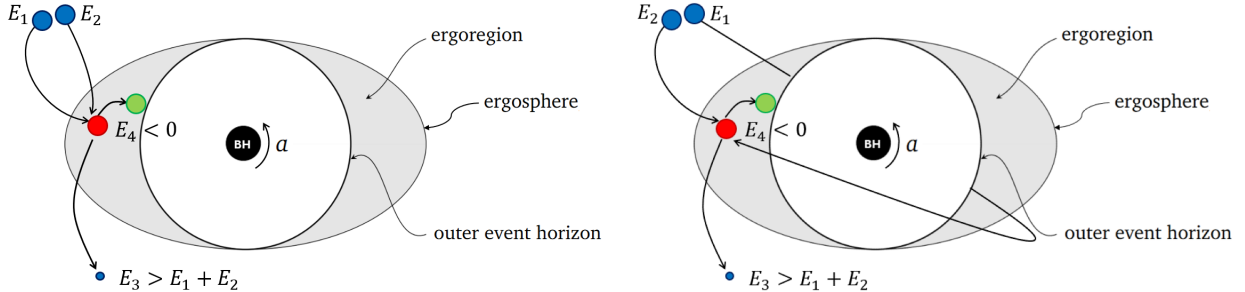


Figure E.1: **Left:** process in which both particles (1) and (2) are *ingoing*. **Right:** process in which particle (1) is *outgoing* and particle (2) is *ingoing*. Reproduced from [42].

On the other hand, we have the polar component

$$p^\theta = \frac{\epsilon^\theta}{\rho^2} \sqrt{Q - \cos^2(\theta) \left(\frac{\ell^2}{\sin^2(\theta)} - a^2(E^2 - m_0^2) \right)} \quad \text{where} \quad \epsilon^\theta = \pm 1. \quad (\text{E.2})$$

Later, we will define the particle's impact parameter

$$b \equiv \frac{\ell}{E}, \quad (\text{E.3})$$

where ℓ and E are the particle's angular momentum and energy, respectively. A particle has a point where it changes direction radially, and at this point, the potential is zero. For photons in the equatorial plane it adopts the following form [52]

$$b_\pm(r) = \frac{2Ma \pm \sqrt{r^4 - 2Mr^3 + (ar)^2}}{2M - r}. \quad (\text{E.4})$$

¹We refer to a particle that comes from infinity and heads towards the event horizon.

²The particle skirts the BH and collides at the event horizon when it is "exiting" the BH.

A massive particle or photon needs an impact parameter of $b = 2$ to approach the horizon as nearly as possible without being deviated. This specific value is known as the *critical impact parameter*. A particle with $b = 2$ is termed critical, whereas a particle with $b < 2$ is referred to as subcritical [42].

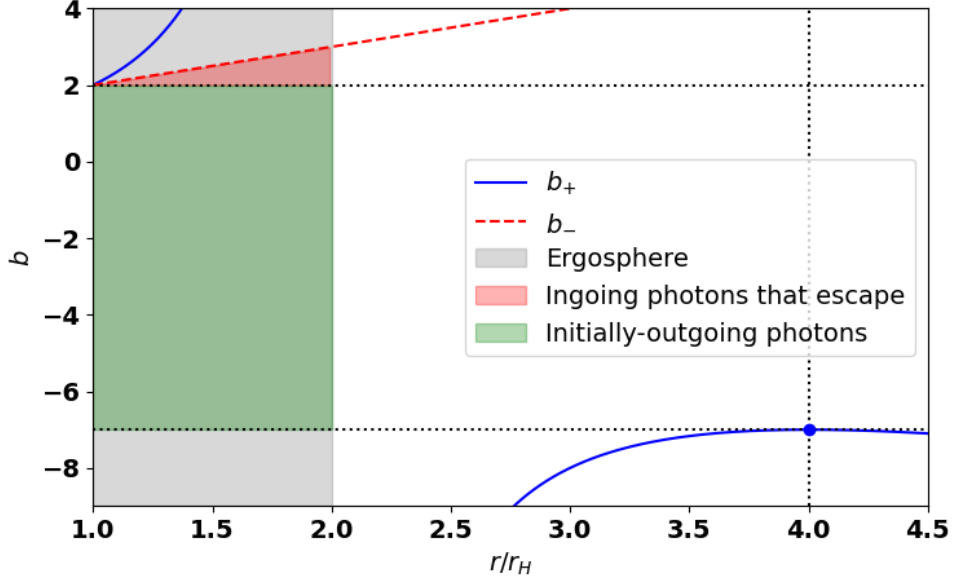


Figure E.2: Conditions of the photon impact parameter $b = b = \ell/E$ near a BH with $a = 1$. The graph illustrates regions where photons can escape or be captured based on their impact parameters and radial positions. Reproduced from [52].

Figure E.2 shows the impact parameters b_+ (blue curve) and b_- (red curve) for photons in the equatorial plane of a BH with $a = 1$. The impact parameter, defined as $b = \ell/E$, represents the ratio between the particle's angular momentum and energy, which is crucial for understanding how photons behave near the event horizon.

The gray-shaded area indicates the ergosphere, extending from $r = 1$ to $r = 2$, where particles cannot remain stationary due to the frame-dragging effect of the rotating BH. The red-shaded region highlights ingoing photons that can escape, while the green area shows initially outgoing photons. These shaded regions illustrate the possible photon trajectories depending on their impact parameters.

As we mentioned before, photons and massive particles with $b = 2$ are considered critical, positioned at the threshold between escaping or being captured by the BH.

Now, if we have a collision of two particles (let's call them 1 and 2) that produce two other particles (continuing with the notation, 3 and 4). The third particle will escape to infinity, while the fourth will fall into the BH as long as there is an increase in energy

$$E_3 > E_1 + E_2 \rightarrow E_4 < 0. \quad (\text{E.5})$$

In the system, we have a series of conserved quantities related to energy and angular momentum.

$$E_{\text{total}} \equiv E_1 + E_2 = E_3 + E_4, \quad \ell_{\text{total}} \equiv b_1 E_1 + b_2 E_2 = b_3 E_3 + b_4 E_4, \quad (\text{E.6})$$

and to the momentum

$$p_{\text{total}}^r \equiv \epsilon_1 p_1^r + \epsilon_2 p_2^r = \epsilon_3 p_3^r + \epsilon_4 p_4^r, \quad p_{\text{total}}^\theta \equiv \epsilon_1 p_1^\theta + \epsilon_2 p_2^\theta = \epsilon_3 p_3^\theta + \epsilon_4 p_4^\theta. \quad (\text{E.7})$$

We also have an effective mass

$$M_{COM}^2 = \frac{E_{total}^2 \left(r^4 + (a^2 - b_{total}^2) r^2 + \Delta \cos^2(\theta) \left(\frac{b_{total}^2}{\sin^2(\theta)} - a^2 \right) + 2r(b_{total} - a)^2 \right) - \rho^4 \left((p_{total}^r)^2 + \Delta (p_{total}^\theta)^2 \right)}{\Delta \rho^2}. \quad (\text{E.8})$$

$$(E.9)$$

On the other hand, we would like to find the energy of the particle that will escape to infinity. To do this, we define the relation

$$Q_3 = \lambda_3^2 E_3^2 \geq \lambda_{3,0}^2 E_3^2, \quad (\text{E.10})$$

where

$$\lambda^2(\theta) \equiv \cos^2(\theta) \left(\frac{b^2}{\sin^2(\theta)} - 1 + \alpha^2 \right) + (\tilde{p}^\theta)^2, \quad \lambda_0^2(\theta) \equiv \cos^2(\theta) \left(\frac{b^2}{\sin^2(\theta)} - 1 + \alpha^2 \right), \quad (\text{E.11})$$

and

$$\tilde{p}^\theta \equiv \frac{\rho^2 p^\theta}{E}, \quad \alpha \equiv \frac{m_0}{E}, \quad (\text{E.12})$$

transforming equation (E.1) in

$$p_3^r = \epsilon_3 \nu_3 E_3, \quad \text{with} \quad \nu = \sqrt{\frac{r^4 - (b^2 - 1)r^2 + 2(b - 1)^2 r - (\lambda^2 + \alpha^2 r^2)\Delta}{\rho^4}} \quad (\text{E.13})$$

Finally, it is necessary to define the Q_N term

$$Q_N \equiv (\rho^2 p_{total}^\theta)^2 + \cos^2(\theta) \left(\frac{\ell_{total}^2}{\sin^2(\theta)} - E_{total}^2 + m_4^2 \right). \quad (\text{E.14})$$

Using the set of equations (E.6) and (E.7), we get rid of the terms of particle (4) and can isolate the energy of the particle that escapes to infinity

$$E_3(E_{total}, \ell_{total}, p_{total}^r, p_{total}^\theta, b_3, p_3^\theta, m_4, r, \theta) = \frac{E_{tot} \rho^2 \Delta (M_{COM}^2 - m_4^2)}{2(E_{tot}^2 r^4 - (b_3 \ell_{tot} E_{tot} - E_{tot}^2) r^2 + 2((b_3 E_{tot} - E_{tot})(\ell_{tot} - E_{tot})) r - Q_D \Delta - \rho^4 p_{tot}^r \epsilon_3 \nu_3 E_{tot})}$$

$$= \frac{E_{tot} [E_{tot}^2 r^4 - (\ell_{tot}^2 - E_{tot}^2) r^2 + 2(\ell_{tot} - E_{tot})^2 r - (m_4^2 r^2 + Q_N) \Delta - (\rho^2 p_{tot}^r)^2]}{2(E_{tot}^2 r^4 - (b_3 \ell_{tot} E_{tot} - E_{tot}^2) r^2 + 2((b_3 E_{tot} - E_{tot})(\ell_{tot} - E_{tot})) r - Q_D \Delta - \rho^4 p_{tot}^r \epsilon_3 \nu_3 E_{tot})}, \quad (\text{E.15})$$

where Q_D is defined as

$$Q_D \equiv \tilde{p}_3^\theta E_{total} p_{total}^\theta + \cos^2(\theta) \left(\frac{b_3 E_{total} \ell_{total}}{\sin^2(\theta)} - E_{total}^2 \right). \quad (\text{E.16})$$

However, it is still possible to achieve a higher maximum efficiency if we take the limit when r tends to 1 over the energy of the third particle (E.15). If we do so, we obtain that

$$E_{3,r \rightarrow 1}(E_1, m_1, \tilde{p}_1^\theta, \tilde{p}_3^\theta, \sin(\theta), b_3 = 2) = \frac{2E_1 \sin(\theta) + \epsilon_1 \sqrt{(m_1^2 - E_1^2) \sin^4(\theta) + (8E_1^2 - 2m_1^2 - E_1^2 (\tilde{p}_1^\theta)^2) \sin^2(\theta) - 4E_1^2}}{2 \sin(\theta) - \sqrt{-\sin^4(\theta) + (8 - (\tilde{p}_3^\theta)^2) \sin^2(\theta) - 4}}. \quad (\text{E.17})$$



Maximal energies and efficiencies for escaping massless particle's cases

F.1 Outgoing pair annihilation (MMP+)

In the MMP+ case ($E_1 = m_1 = \epsilon_1 = 1$ and $\tilde{p}_1^\theta = \tilde{p}_3^\theta = 0$)

$$E_{3,r \rightarrow 1}(\tilde{p}_1^\theta, \tilde{p}_3^\theta, \sin(\theta)) = \frac{2 \sin(\theta) + \sqrt{(6 - (\tilde{p}_1^\theta)^2) \sin^2(\theta) - 4}}{2 \sin(\theta) - \sqrt{-\sin^4(\theta) + (8 - (\tilde{p}_3^\theta)^2) \sin^2(\theta) - 4}}. \quad (\text{F.1})$$

Substituting $\tilde{p}_1^\theta = \tilde{p}_3^\theta = 0$ we find that

$$E_{3,r \rightarrow 1}(\sin(\theta)) = \frac{2 \sin(\theta) + \sqrt{6 \sin^2(\theta) - 4}}{2 \sin(\theta) - \sqrt{-\sin^4(\theta) + 8 \sin^2(\theta) - 4}}. \quad (\text{F.2})$$

Now, assuming the [eq. plane](#)

$$\boxed{E_{3,r \rightarrow 1} = \frac{2 + \sqrt{6 - 4}}{2 - \sqrt{-1 + 8 - 4}} = \frac{2 + \sqrt{2}}{2 - \sqrt{3}} \approx 12.74}. \quad (\text{F.3})$$

The efficiency is then

$$\boxed{\eta_{MMP+} = \frac{E_3}{E_1 + E_2} = \left(\frac{2 + \sqrt{2}}{2 - \sqrt{3}} \right) \left(\frac{1}{1 + 1} \right) = \frac{2 + \sqrt{2}}{2(2 - \sqrt{3})} \approx 6.37} \quad (\text{F.4})$$

F.2 Ingoing Compton Scattering (PMP-)

For the PMP- ($m_1 = 0, \epsilon_1 = -1, \max(\tilde{p}_1^\theta)$ y $\tilde{p}_3^\theta = 0$):

$$E_{3,r \rightarrow 1}(\tilde{p}_1^\theta, \tilde{p}_3^\theta, \sin(\theta)) = \frac{2E_1 \sin(\theta) - \sqrt{(-E_1^2) \sin^4(\theta) + (8E_1^2 - E_1^2(\tilde{p}_1^\theta)^2) \sin^2(\theta) - 4E_1^2}}{2 \sin(\theta) - \sqrt{-\sin^4(\theta) + (8 - (\tilde{p}_3^\theta)^2) \sin^2(\theta) - 4}}. \quad (\text{F.5})$$

The maximum of \tilde{p}_1^θ cancels the root and $\tilde{p}_3^\theta = 0$

$$E_{3,r \rightarrow 1}(\sin(\theta)) = \frac{2E_1 \sin(\theta)}{2 \sin(\theta) - \sqrt{-\sin^4(\theta) + 8 \sin^2(\theta) - 4}}, \quad (\text{F.6})$$

which, in the [eq. plane](#), results in

$$E_{3,r \rightarrow 1} = \frac{2E_1}{2 - \sqrt{-1 + 8 - 4}} = \frac{2E_1}{2 - \sqrt{3}} \approx 7.46E_1. \quad (\text{F.7})$$

The efficiency results then in

$$\eta_{PMP-} = \lim_{E_1 \rightarrow \infty} \frac{2E_1}{(2 + \sqrt{3})(E_1 + 1)} = \frac{\infty}{\infty}. \quad (\text{F.8})$$

We need to divide both the numerator and denominator by E_1

$$2(2 + \sqrt{3}) \lim_{E_1 \rightarrow \infty} \frac{1}{\frac{1}{E_1} + 1}. \quad (\text{F.9})$$

The $\frac{1}{E_1}$ terms tend to zero when $E_1 \rightarrow \infty$

$$2(2 + \sqrt{3}) \lim_{E_1 \rightarrow \infty} \frac{1}{\frac{0}{\frac{1}{E_1}} + 1} = 2(2 + \sqrt{3}) \lim_{E_1 \rightarrow \infty} \frac{1}{1}. \quad (\text{F.10})$$

The limit of a constant is also a constant

$$\eta_{PMP-} = 2(2 + \sqrt{3}) \lim_{E_1 \rightarrow \infty} \frac{1}{1} = 2(2 + \sqrt{3}) \approx 7.46. \quad (\text{F.11})$$

F.3 Outgoing Compton Scattering (PMP+)

Now for the PMP+ case ($m_1 = 0$, $\epsilon_1 = +1$ and $\tilde{p}_1^\theta = \tilde{p}_3^\theta = 0$.)

$$E_{3,r \rightarrow 1}(\tilde{p}_1^\theta, \tilde{p}_3^\theta, \sin(\theta)) = \frac{2E_1 \sin(\theta) + \sqrt{(-E_1^2) \sin^4(\theta) + (8E_1^2 - E_1^2(\tilde{p}_1^\theta)^2) \sin^2(\theta) - 4E_1^2}}{2 \sin(\theta) - \sqrt{-\sin^4(\theta) + (8 - (\tilde{p}_3^\theta)^2) \sin^2(\theta) - 4}}. \quad (\text{F.12})$$

Substituting $\tilde{p}_1^\theta = \tilde{p}_3^\theta = 0$:

$$E_{3,r \rightarrow 1}(\sin(\theta)) = \frac{2E_1 \sin(\theta) + \sqrt{(-E_1^2) \sin^4(\theta) + 8E_1^2 \sin^2(\theta) - 4E_1^2}}{2 \sin(\theta) - \sqrt{-\sin^4(\theta) + 8 \sin^2(\theta) - 4}}. \quad (\text{F.13})$$

Assuming that the process is occurring in the [eq. plane](#)

$$E_{3,r \rightarrow 1} = \frac{2E_1 + \sqrt{-E_1^2 + 8E_1^2 - 4E_1^2}}{2 - \sqrt{-1 + 8 - 4}} = \frac{2E_1 + \sqrt{3E_1^2}}{2 - \sqrt{3}} = E_1(7 + 4\sqrt{3}) \approx 13.92E_1. \quad (\text{F.14})$$

The efficiency will have a value of

$$\eta_{PMP-} = \frac{E_1(7 + 4\sqrt{3})}{E_1 - 1}. \quad (\text{F.15})$$

We test what happens when E_1 tends to ∞ :

$$\lim_{E_1 \rightarrow \infty} \frac{E_1(7 + 4\sqrt{3})}{E_1 - 1} = \frac{\infty}{\infty}. \quad (\text{F.16})$$

We need to divide both the numerator and denominator by E_1

$$(7 + 4\sqrt{3}) \lim_{E_1 \rightarrow \infty} \frac{1}{1 - \frac{1}{E_1}}. \quad (\text{F.17})$$

The $\frac{1}{E_1^n}$ terms tend to zero when $E_1 \rightarrow \infty$, so

$$(7 + 4\sqrt{3}) \lim_{E_1 \rightarrow \infty} \frac{1}{1}. \quad (\text{F.18})$$

Then

$$\boxed{\eta_{PMP+} = 7 + 4\sqrt{3} \approx 13.92}. \quad (\text{F.19})$$

F.4 Ingoing inverse Compton scattering (MPP-)

In this process ($E_1 = m_1 = 1, \epsilon_1 = -1, \max(\tilde{p}_1^\theta) \text{ y } \tilde{p}_3^\theta = 0$):

$$E_{3,r \rightarrow 1}(\tilde{p}_1^\theta, \tilde{p}_3^\theta, \sin(\theta)) = \frac{2 \sin(\theta) - \sqrt{(6 - (\tilde{p}_1^\theta)^2) \sin^2(\theta) - 4}}{2 \sin(\theta) - \sqrt{-\sin^4(\theta) + (8 - (\tilde{p}_3^\theta)^2) \sin^2(\theta) - 4}}. \quad (\text{F.20})$$

The maximum of \tilde{p}_1^θ will cancel the root, and we also have that $\tilde{p}_3^\theta = 0$, therefore

$$E_{3,r \rightarrow 1}(\sin(\theta)) = \frac{2 \sin(\theta)}{2 \sin(\theta) - \sqrt{-\sin^4(\theta) + 8 \sin^2(\theta) - 4}}. \quad (\text{F.21})$$

The eq. plane will simplify it to

$$\boxed{E_{3,r \rightarrow 1} = \frac{2}{2 - \sqrt{-1 + 8 - 4}} = \frac{2}{2 - \sqrt{3}} = 4 + 2\sqrt{3} \approx 7.46}. \quad (\text{F.22})$$

The efficiency will take the value of

$$\boxed{\eta_{MPP-} = \frac{E_3}{E_1 + E_2} = \left. \frac{4 + 2\sqrt{3}}{1 + E_2} \right|_{E_2 \rightarrow 0} = 4 + 2\sqrt{3} \approx 7.46}.$$

F.5 Outgoing inverse Compton scattering (MPP+)

Here we will have ($E_1 = m_1 = \epsilon_1 = +1 \text{ y } \tilde{p}_1^\theta = \tilde{p}_3^\theta = 0$)

$$E_{3,r \rightarrow 1}(\tilde{p}_1^\theta, \tilde{p}_3^\theta, \sin(\theta)) = \frac{2 \sin(\theta) + \sqrt{(6 - (\tilde{p}_1^\theta)^2) \sin^2(\theta) - 4}}{2 \sin(\theta) - \sqrt{-\sin^4(\theta) + (8 - (\tilde{p}_3^\theta)^2) \sin^2(\theta) - 4}}. \quad (\text{F.23})$$

Substituting $\tilde{p}_1^\theta = \tilde{p}_3^\theta = 0$

$$E_{3,r \rightarrow 1}(\sin(\theta)) = \frac{2 \sin(\theta) + \sqrt{6 \sin^2(\theta) - 4}}{2 \sin(\theta) - \sqrt{-\sin^4(\theta) + 8 \sin^2(\theta) - 4}}. \quad (\text{F.24})$$

If we position ourselves in the eq. plane

$$E_{3,r \rightarrow 1} = \frac{2 + \sqrt{6 - 4}}{2 - \sqrt{-1 + 8 - 4}} = \frac{2 + \sqrt{2}}{2 - \sqrt{3}} \approx 12.74 , \quad (\text{F.25})$$

resulting in an efficiency of

$$\eta_{MPP+} = \frac{E_3}{E_1 + E_2} = \left(\frac{2 + \sqrt{2}}{2 - \sqrt{3}} \right) \frac{1}{E_1 + E_2} \Big|_{E_2 \rightarrow 0} = \frac{2 + \sqrt{2}}{2 - \sqrt{3}} \approx 12.74 . \quad (\text{F.26})$$

G

Maximal energies and efficiencies for escaping massive particle's cases

G.1 Ingoing elastic scattering (MMM-)

For MMM- ($E_1 = m_1 = 1$, $\epsilon = -1$ y $\max(\tilde{p}_1^\theta)$):

$$E_{3,r \rightarrow 1}(\tilde{p}_1^\theta, \sin(\theta), \alpha_3) = \frac{2E_1 \sin(\theta) - \sqrt{(m_1^2 - E_1^2) \sin^4(\theta) + (8E_1^2 - 2m_1^2 - E_1^2(\tilde{p}_1^\theta)^2) \sin^2(\theta) - 4E_1^2}}{2 \sin(\theta) - \sqrt{8 \sin^2(\theta) - \sin^4(\theta) - 4 - \alpha_3^2(2 \sin^2(\theta) - \sin^4(\theta))}}. \quad (\text{G.1})$$

The maximum of the function \tilde{p}_1^θ cancels the square root:

$$E_{3,r \rightarrow 1}(\sin(\theta), \alpha_3) = \frac{2 \sin(\theta)}{2 \sin(\theta) - \sqrt{8 \sin^2(\theta) - \sin^4(\theta) - 4 - \alpha_3^2(2 \sin^2(\theta) - \sin^4(\theta))}}. \quad (\text{G.2})$$

In the [eq. plane](#)

$$E_{3,r \rightarrow 1}(\alpha_3) = \frac{2}{2 - \sqrt{3 - \alpha_3^2}}, \quad (\text{G.3})$$

and, as $E_3 = 1/\alpha_3$,

$$\frac{1}{\alpha_3} = \frac{2}{2 - \sqrt{3 - \alpha_3^2}} \rightarrow \alpha_3 = \frac{4 - \sqrt{11}}{5}. \quad (\text{G.4})$$

Substituting this we obtain

$$E_{3,r \rightarrow 1} = \frac{2}{2 - \sqrt{3 - \left(\frac{4 - \sqrt{11}}{5}\right)^2}} = 4 + \sqrt{11} \approx 7.32. \quad (\text{G.5})$$

Then, the efficiency results in

$$\eta_{\text{MMM-}} = \frac{E_3}{E_1 + E_2} = \frac{4 + \sqrt{11}}{1 + 1} = \frac{4 + \sqrt{11}}{2} \approx 3.66. \quad (\text{G.6})$$

G.2 Ingoing inverse Compton scattering (MPM-)

In the MPM- process ($E_1 = m_1 = 1$, $\epsilon = -1$ y $\max(\tilde{p}_1^\theta)$):

$$E_{3,r \rightarrow 1}(\tilde{p}_1^\theta, \sin(\theta), \alpha_3) = \frac{2E_1 \sin(\theta) - \sqrt{(m_1^2 - E_1^2) \sin^4(\theta) + (8E_1^2 - 2m_1^2 - E_1^2(\tilde{p}_1^\theta)^2) \sin^2(\theta) - 4E_1^2}}{2 \sin(\theta) - \sqrt{8 \sin^2(\theta) - \sin^4(\theta) - 4 - \alpha_3^2(2 \sin^2(\theta) - \sin^4(\theta))}}. \quad (\text{G.7})$$

The maximum of the function \tilde{p}_1^θ cancels the square root:

$$E_{3,r \rightarrow 1}(\sin(\theta), \alpha_3) = \frac{2 \sin(\theta)}{2 \sin(\theta) - \sqrt{8 \sin^2(\theta) - \sin^4(\theta) - 4 - \alpha_3^2(2 \sin^2(\theta) - \sin^4(\theta))}}. \quad (\text{G.8})$$

In the [eq. plane](#)

$$E_{3,r \rightarrow 1}(\alpha_3) = \frac{2}{2 - \sqrt{3 - \alpha_3^2}}, \quad (\text{G.9})$$

and, as $E_3 = 1/\alpha_3$,

$$\frac{1}{\alpha_3} = \frac{2}{2 - \sqrt{3 - \alpha_3^2}} \rightarrow \alpha_3 = \frac{4 - \sqrt{11}}{5}. \quad (\text{G.10})$$

Substituting in (G.9) we obtain

$$E_{3,r \rightarrow 1} = \frac{2}{2 - \sqrt{3 - \left(\frac{4 - \sqrt{11}}{5}\right)^2}} = 4 + \sqrt{11} \approx 7.32. \quad (\text{G.11})$$

Then, the efficiency results in

$$\eta_{MPM-} = \left. \frac{E_3}{E_1 + E_2} \right|_{E_2 \rightarrow 0} = \frac{4 + \sqrt{11}}{1 + 0} = 4 + \sqrt{11} \approx 7.32. \quad (\text{G.12})$$

G.3 Outgoing inverse Compton scattering (MPM+)

The MPM+ process ($E_1 = m_1 = \epsilon = 1$ and $\tilde{p}_1^\theta = 0$):

$$E_{3,r \rightarrow 1}(\tilde{p}_1^\theta, \sin(\theta), \alpha_3) = \frac{2 \sin(\theta) + \sqrt{(6 - (\tilde{p}_1^\theta)^2) \sin^2(\theta) - 4}}{2 \sin(\theta) - \sqrt{8 \sin^2(\theta) - \sin^4(\theta) - 4 - \alpha_3^2(2 \sin^2(\theta) - \sin^4(\theta))}}. \quad (\text{G.13})$$

Here, the function $\tilde{p}_1^\theta = 0$

$$E_{3,r \rightarrow 1}(\sin(\theta), \alpha_3) = \frac{2 \sin(\theta) + \sqrt{6 \sin^2(\theta) - 4}}{2 \sin(\theta) - \sqrt{8 \sin^2(\theta) - \sin^4(\theta) - 4 - \alpha_3^2(2 \sin^2(\theta) - \sin^4(\theta))}}. \quad (\text{G.14})$$

If we consider that the process occurs in the [eq. plane](#)

$$E_{3,r \rightarrow 1}(\alpha_3) = \frac{2 + \sqrt{6 - 4}}{2 - \sqrt{8 - 1 - 4 - \alpha_3^2(2 - 1)}} = \frac{2 + \sqrt{2}}{2 - \sqrt{3 - \alpha_3^2}}, \quad (\text{G.15})$$

and we know that $E_3 = 1/\alpha_3$

$$\frac{1}{\alpha_3} = \frac{2 + \sqrt{2}}{2 - \sqrt{3 - \alpha_3^2}} \rightarrow \alpha_3 = \frac{7 - 4\sqrt{2}}{17}. \quad (\text{G.16})$$

This results in the following energy

$$E_{3,r \rightarrow 1} = \frac{2}{2 - \sqrt{3 - \left(\frac{7-4\sqrt{2}}{17}\right)^2}} = 7 + 4\sqrt{2} \approx 12.66, \quad (\text{G.17})$$

that transforms the efficiency as

$$\eta_{PMM+} = \left. \frac{E_3}{E_1 + E_2} \right|_{E_2 \rightarrow 0} = \frac{7 + 4\sqrt{2}}{1 + 0} = 7 + 4\sqrt{2} \approx 12.66. \quad (\text{G.18})$$

G.4 Ingoing photomeson production (PMM-)

The PMM- case ($m_1 = 1$, $\epsilon = -1$ y $\max(\tilde{p}_1^\theta)$)

$$E_{3,r \rightarrow 1}(\tilde{p}_1^\theta, \sin(\theta), \alpha_3) = \frac{2E_1 \sin(\theta) - \sqrt{(1-E_1^2)\sin^4(\theta) + (8E_1^2 - 2 - E_1^2(\tilde{p}_1^\theta)^2)\sin^2(\theta) - 4E_1^2}}{2 \sin(\theta) - \sqrt{8\sin^2(\theta) - \sin^4(\theta) - 4 - \alpha_3^2(2\sin^2(\theta) - \sin^4(\theta))}}. \quad (\text{G.19})$$

The maximum of \tilde{p}_1^θ cancels the square root resulting in

$$E_{3,r \rightarrow 1}(\sin(\theta), \alpha_3) = \frac{2E_1 \sin(\theta)}{2 \sin(\theta) - \sqrt{8\sin^2(\theta) - \sin^4(\theta) - 4 - \alpha_3^2(2\sin^2(\theta) - \sin^4(\theta))}}. \quad (\text{G.20})$$

When the interaction occurs in the [eq. plane](#)

$$E_{3,r \rightarrow 1}(\alpha_3) = \frac{2E_1}{2 - \sqrt{3 - \alpha_3^2}}, \quad (\text{G.21})$$

and, as $E_3 = 1/\alpha_3$,

$$\frac{1}{\alpha_3} = \frac{2E_1}{2 - \sqrt{3 - \alpha_3^2}} \rightarrow \alpha_3 = \frac{8E_1 \pm \sqrt{48E_1^2 - 4}}{8E_1^2 + 2}. \quad (\text{G.22})$$

This can be substituted in (G.21) obtaining

$$E_{3,r \rightarrow 1} = \frac{2E_1}{2 - \sqrt{3 - \left(\frac{8E_1 \pm \sqrt{48E_1^2 - 4}}{8E_1^2 + 2}\right)^2}} = 4E_1 + \sqrt{12E_1^2 - 1}. \quad (\text{G.23})$$

So, the efficiency takes the following form

$$\eta_{PMM-} = \left. \frac{E_3}{E_1 + E_2} \right|_{E_1 \rightarrow \infty} = \lim_{E_1 \rightarrow \infty} \frac{4E_1 + \sqrt{12E_1^2 - 1}}{E_1 + 1} = \frac{\infty}{\infty} \quad (\text{G.24})$$

We divide the numerator and the denominator by E_1 :

$$\lim_{E_1 \rightarrow \infty} \frac{4 + \sqrt{12 - \frac{1}{E_1^2}}}{\frac{1}{E_1} + 1} \quad (\text{G.25})$$

The terms $1/E_1^n$ tend to zero as $E_1 \rightarrow \infty$:

$$\lim_{E_1 \rightarrow \infty} \frac{4 + \sqrt{12 - \frac{1}{E_1^2}}}{\frac{1}{E_1} + 1} = \frac{4 + 2\sqrt{3}}{1}. \quad (\text{G.26})$$

This results in

$$\boxed{\eta_{PMM-} = 4 + 2\sqrt{3} \approx 7.46}.$$

G.5 Outgoing photomeson production (PMM+)

The PMM+ interaction ($m_1 = \epsilon = 1$ y $\tilde{p}_1^\theta = 0$):

$$E_{3,r \rightarrow 1}(\tilde{p}_1^\theta, \sin(\theta), \alpha_3) = \frac{2E_1 \sin(\theta) - \sqrt{(1-E_1^2)\sin^4(\theta) + (8E_1^2 - 2 - E_1^2(\tilde{p}_1^\theta)^2)\sin^2(\theta) - 4E_1^2}}{2 \sin(\theta) - \sqrt{8\sin^2(\theta) - \sin^4(\theta) - 4 - \alpha_3^2(2\sin^2(\theta) - \sin^4(\theta))}}. \quad (\text{G.27})$$

When inserting $\tilde{p}_1^\theta = 0$ we find that

$$E_{3,r \rightarrow 1}(\sin(\theta), \alpha_3) = \frac{2E_1 \sin(\theta) + \sqrt{(1-E_1^2)\sin^4(\theta) + (8E_1^2 - 2)\sin^2(\theta) - 4E_1^2}}{2 \sin(\theta) - \sqrt{8\sin^2(\theta) - \sin^4(\theta) - 4 - \alpha_3^2(2\sin^2(\theta) - \sin^4(\theta))}} \quad (\text{G.28})$$

Assuming the eq. plane

$$E_{3,r \rightarrow 1}(\alpha_3) = \frac{2E_1 + \sqrt{3E_1^2 - 1}}{2 - \sqrt{3 - \alpha_3^2}} \quad (\text{G.29})$$

and knowing that $E_3 = 1/\alpha_3$

$$\frac{1}{\alpha_3} = \frac{2E_1 + \sqrt{3E_1^2 - 1}}{2 - \sqrt{3 - \alpha_3^2}} \rightarrow \alpha_3 = \frac{4(2E_1 + \sqrt{3E_1^2 - 1}) \pm \sqrt{(4(2E_1 + \sqrt{3E_1^2 - 1}))^2 - 4(2E_1 + \sqrt{3E_1^2 - 1}) + 1}}{2((2E_1 + \sqrt{3E_1^2 - 1}) + 1)}. \quad (\text{G.30})$$

We can find now the energy

$$\boxed{E_3 = (4 + 2\sqrt{3})E_1 + \sqrt{(3(7 + 4\sqrt{3})^2 E_1^2 - 1)}}, \quad (\text{G.31})$$

and find the efficiency following the same procedure as before

$$\eta_{PMM+} = \left. \frac{E_3}{E_1 + E_2} \right|_{E_1 \rightarrow \infty} = \lim_{E_1 \rightarrow \infty} \frac{2(2 + \sqrt{3})E_1 + \sqrt{(3(2 + \sqrt{3})^2 E_1^2 - 1)}}{E_1 + 1} = \frac{\infty}{\infty}. \quad (\text{G.32})$$

First, we will divide the numerator and the denominator by E_1 :

$$\lim_{E_1 \rightarrow \infty} \frac{2(2 + \sqrt{3}) + \sqrt{(3(2 + \sqrt{3})^2 - \frac{1}{E_1^2})}}{\frac{1}{E_1} + 1} \quad (\text{G.33})$$

The terms $1/E_1^n$ tend to zero as $E_1 \rightarrow \infty$:

$$\lim_{E_1 \rightarrow \infty} \frac{2(2 + \sqrt{3}) + \sqrt{\left(3(2 + \sqrt{3})^2 - \frac{1}{E_1^2}\right)^0}}{\frac{1}{E_1} + 1}, \quad (\text{G.34})$$

resulting in

$$\boxed{\eta_{PMM+} = 2(2 + \sqrt{3}) + \sqrt{3(2 + \sqrt{3})^2} \approx 13.92}.$$